

The Astrophysical Journal, in press

Are Coronae of Magnetically Active Stars Heated by Flares? II. EUV and X-Ray Flare Statistics and the Differential Emission Measure Distribution

Manuel Güdel and Marc Audard¹

Paul Scherrer Institut, Würenlingen and Villigen, CH-5232 Villigen PSI, Switzerland

guedel@astro.phys.ethz.ch, audard@astro.columbia.edu

Vinay L. Kashyap and Jeremy J. Drake

*Harvard-Smithsonian Center for Astrophysics, 60 Garden Street, Cambridge, MA 02138,
USA*

vkashyap@cfa.harvard.edu, jdrake@cfa.hardvard.edu

and

Edward F. Guinan

*Department of Astronomy and Astrophysics, Villanova University, Villanova, PA 19085,
USA*

edward.guinan@villanova.edu

ABSTRACT

We investigate the EUV and X-ray flare rate distribution in radiated energy of the late-type active star AD Leo. Occurrence rates of *solar* flares have previously been found to be distributed in energy according to a power law, $dN/dE \propto E^{-\alpha}$, with a power-law index α in the range 1.5–2.6. If $\alpha \geq 2$, then an extrapolation of the flare distribution to low flare energies may be sufficient to heat the complete observable X-ray/EUV corona.

¹Present address: Columbia Astrophysics Laboratory, Columbia University, 550 West 120th Street, New York, NY 10027, USA

We have obtained long observations of AD Leo with the *EUVE* and *BeppoSAX* satellites. Numerous flares have been detected, ranging over almost two orders of magnitude in their radiated energy. We compare the observed light curves with light curves synthesized from model flares that are distributed in energy according to a power law with selectable index α . Two methods are applied, the first comparing flux distributions of the binned data, and the second using the distributions of photon arrival time differences in the unbinned data (for *EUVE*). Subsets of the light curves are tested individually, and the quiescent flux has optionally been treated as a superposition of flares from the same flare distribution. We find acceptable α values between 2.0–2.5 for the *EUVE* DS and the *BeppoSAX* LECS data. Some variation is found depending on whether or not a strong and long-lasting flare occurring in the *EUVE* data is included. The *BeppoSAX* MECS data indicate a somewhat shallower energy distribution (smaller α) than the simultaneously observed LECS data, which is attributed to the harder range of sensitivity of the MECS detector and the increasing peak temperatures of flares with increasing total (radiative) energy. The results suggest that flares can play an important role in the energy release of this active corona. We discuss caveats related to time variability, total energy, and multiple power-law distributions. Studying the limiting case of a corona that is entirely heated by a population of flares, we derive an expression for the time-averaged coronal differential emission measure distribution (DEM) that can be used as a diagnostic for the flare energy distribution. The shape of the analytical DEM agrees with previously published DEMs from observations of active stars.

Subject headings: Stars: activity—stars: coronae—stars: flare—stars: individual (AD Leo)—stars: late-type

1. Introduction

The physics of coronal heating remains one of the most fundamental problems in stellar (and solar) astrophysics. The subject has been reviewed extensively from the point of view of theoretical concepts (Ionson 1985; Narain & Ulmschneider 1990; Zirker 1993), observational solar physics (e.g., Benz 1994), and stellar physics (e.g., Haisch & Schmitt 1996), where the cited work stands exemplary for a large body of literature available. It is somewhat surprising that the nature of the “coronal heating mechanism(s)” still eludes agreement given high-resolution imaging of solar coronal structures or large statistical samples of stellar coronal X-ray observations. For example, there is no unequivocal agreement on whether all, or any,

of the X-ray coronal energy detected from *certain* classes of stars is magnetic in origin.

Coronal heating is of particular interest to stellar astrophysics since it relates directly to our understanding of coronal structure and dynamics, information that is usually obtained by means of indirect modeling. Apart from heating models involving acoustic heating, for example on F-type stars (see Mullan & Cheng 1994; although the resulting X-ray flux would be much smaller than observed - see Stępień & Ulmschneider 1989), the currently advocated mechanisms are of two types: (i) Steady heating mechanisms, e.g., by steady electric current dissipation or MHD waves, and (ii) heating by explosive energy release, e.g., coronal flares. The latter are attractive heating agents since flares do heat plasma efficiently, although only episodically since the radiative and conductive losses rapidly cool plasma to pre-flare levels, typically within minutes to hours.

The flare heating hypothesis has gained momentum in particular from solar, but also from stellar observations during recent years. If the quasi-steady (“quiescent”) coronal emission is to be explained by flare contributions, flares must act as *stochastic* heating agents. Parker (1988) proposed that shuffling of magnetic field footpoints in the photosphere by the convective motions leads to tangled magnetic field lines in the corona and thus to current sheets. With increasing winding of magnetic fields, the necessary energy may be transported into the coronal magnetic field where it is released by sudden relaxation involving reconnection. Parker estimates that energy dissipation occurs in packets involving $10^{24} - 10^{25}$ ergs (“nanoflares”). The flare-heating hypothesis resolves to the basic question of whether or not the *statistical ensemble* of flares (in time and energy) suffices to heat the apparently nonflaring coronae.

2. Statistical Flare Observations: A Brief Overview

Solar observations have provided evidence for the presence of numerous small-scale flare events occurring in the solar corona at any time (Lin et al. 1984; Porter, Fontenla, & Simnett 1995; Gary, Hartl, & Shimizu 1997; Krucker & Benz 1998). Their distribution in energy was found to be a power law (Datlowe, Elcan, & Hudson 1974; Lin et al. 1984) of the form

$$\frac{dN}{dE} = kE^{-\alpha} \quad (1)$$

where dN is the number of flares (per unit time) with a total energy (thermal or radiated) in the interval $[E, E + dE]$. The power-law index α is crucial: If $\alpha \geq 2$, then the energy integration (for a given time interval),

$$E_{\text{tot}} = \int_{E_{\text{min}}}^{E_{\text{max}}} \frac{dN}{dE} E dE \approx \frac{k}{\alpha - 2} E_{\text{min}}^{-(\alpha-2)} \quad (2)$$

(assuming $E_{\min} \ll E_{\max}$ and $\alpha > 2$ for the last approximation) diverges for $E_{\min} \rightarrow 0$, i.e., by extrapolating the power law to sufficiently small flare energies (microflares with $\sim 10^{27} - 10^{30}$ erg, nanoflares with $\sim 10^{24} - 10^{27}$ erg), *any* energy release power can be attained (Hudson 1991). This is not the case for $\alpha < 2$. Evidently, then, one needs to measure the energy distribution of a statistically relevant number of flares. Solar studies have repeatedly resulted in α values on the order of 1.6–1.8 for ordinary solar flares (Crosby, Aschwanden, & Dennis 1993), insufficient for a coronal microflare-heating model. On the other hand, such values have proven interesting for statistical modeling since they are also found from avalanche models (Lu & Hamilton 1991). However, the implicit assumption is that the same power law continues to very low energies with unchanged α . If α steepens for low energies, then the microflare-heating concept may well be in order (Hudson 1991), and such a steepening is supported by simulations of avalanche models for small events (Vlahos et al. 1995). Detailed studies of small events in the soft X-ray (SXR) and extreme ultraviolet (EUV) ranges with Yohkoh, SoHO, and TRACE still provide a somewhat ambiguous picture (Shimizu 1995; Krucker & Benz 1998; Aschwanden et al. 2000; Parnell & Jupp 2000), although recent statistical investigations suggest $\alpha = 2.0 - 2.6$ for small flares in the quiet solar corona (Krucker & Benz 1998; Parnell & Jupp 2000). An extrapolation to unseen microevents is always required to explain all of the coronal energy release, in some cases by several orders of magnitude. Aschwanden et al. (2000) argued that the extrapolation is limited if small flares follow some scaling laws established at higher energies, i.e., their temperatures drop to sub-coronal values, their densities become unreasonably small, and their surface area filling factor approaches unity possibly above the low-energy limit required.

There are two critical questions to ask here: (i) Is the power-law index of the flare energy distribution different for different flare energy ranges? Even if $\alpha < 2$ for ordinary flares, a steepening at lower energies to $\alpha \geq 2$ can have important consequences for the coronal heating energy budget, and the recent findings for microflares seem to support this hypothesis. (ii) Does the derived power-law index α depend on the spectral range in which the observations were made? Incidentally, the recent microflare observations that result in $\alpha \geq 2$ were mostly obtained in the EUV range where the dominant emission comes from hot plasma. It is by no means evident that the hard X-ray production is proportional to the thermal flare energy (Feldman, Doschek, & Klimchuk 1997), and it is clear that the energy released in the hard X-ray (HXR) range (that has often been used for flare statistics) is a very small fraction of the total flare energy. Heating and particle acceleration systematics in the flare energy release may affect both problem areas: The flare temperature and the production of non-thermal particles systematically depend on the total flare energy (e.g., Feldman, Laming, & Doschek 1995; Porter et al. 1995; Aschwanden 1999; Krucker & Benz 2000). We will address both questions in the course of the present study. A summary of a

few relevant observations of solar flare energy distributions is given in Table 1. A further important problem visible in this table relates to peak flux measurements: These are reliable indicators for the total flare energy only if the flare duration does not depend on the total flare energy (Crosby et al. 1993; Porter et al. 1995).

There has been some interesting progress also on the stellar side. Most of the evidence for an important role of flares relates to *magnetically active* stars with coronal energy loss rates orders of magnitude larger than the Sun’s. Doyle & Butler (1985) and Skumanich (1985) noted that the quiescent coronal X-ray luminosity of active stars, L_X , is correlated with their time-averaged U-band flare luminosity, which may indicate that the statistical ensemble of flares is responsible for the energy deposition in the corona. Analogously, Audard et al. (2000) find that the X-ray flare frequency (above a given energy limit) also correlates with L_X . Wood et al. (1996) interpret broadened ultraviolet-line wings as being due to a large number of transient, explosive events similar to those previously identified in the solar corona (Dere, Bartoe, & Brueckner 1989). Observations of active stars often show slow variability within a factor of 2 over both short and long terms, apart from obvious flaring (Ambruster, Sciortino, & Golub 1987; Collura, Pasquini, & Schmitt 1988; Güdel et al. 1996; Kashyap & Drake 1999; Sciortino et al. 1999). Statistically, the hotter X-ray emitting plasma component is more variable than the cooler one, indicating that flares may be involved (Giampapa et al. 1996). Further, small flare events with energies of the order of $10^{27} - 10^{28}$ ergs have become observable with the Hubble Space Telescope in cool M dwarfs, and some of their energy distributions suggest $\alpha > 2$ (Robinson et al. 1995, 1999, 2001) although we note that these transition region events may not be related to the physics of coronal heating.

Studies of *statistical flare energy distributions* in stellar coronae have been rare, due to the paucity of relevant data sets (Table 1). Collura et al. (1988) and Pallavicini, Tagliaferri, & Stella (1990) derived $\alpha = 1.5 - 1.7$ for a sample of M-dwarf flare observations with EXOSAT, and Osten & Brown (1999) report $\alpha = 1.6$ for a set of flares on RS CVn binary systems observed with *EUVE*. All observations obtained flare energies simply by integrating count rates during flares selected from the light curves. Also, these investigations collected flare information from numerous different stars, regardless of distance (introducing selection bias for small flares), luminosity (and hence overall magnetic activity level), binarity, etc. To avoid possible selection bias, Audard, Güdel, & Guinan (1999) and Audard et al. (2000) applied a flare search algorithm to *EUVE* light curves of individual active main-sequence stars, taking into account flare superpositions and various binning to recognize weak flares. Although the statistical confidence intervals are broad, the results indicate a predominance of relatively steep power laws including $\alpha \geq 2$, suggesting that the extension of the flare distribution to lower energies may contribute considerably to the detected energy loss.

Table 1. PREVIOUS MEASUREMENTS OF FLARE ENERGY DISTRIBUTIONS
(SELECTION)

Measurement	Photon energy range	Flare energy	α	Reference
<i>Solar:</i>				
Thermal energy	EUV Fe IX, X, XII	$10^{25} - 3 \times 10^{26}$ erg	2.3–2.6	Krucker & Benz 1998
Thermal energy	EUV Fe IX, X, XII	$3 \times 10^{23} - 10^{26}$ erg	2.0–2.6	Parnell & Jupp 2000
Thermal energy	EUV Fe IX, X, XII	$10^{24} - 2 \times 10^{26}$ erg	1.79 ± 0.08	Aschwanden et al. 2000
Thermal and radiated energy	SXR	$10^{27} - 10^{29}$ erg	1.5–1.6	Shimizu 1995
Peak flux	SXR	$10^{25} - 10^{29}$ erg	1.4–1.8	Shimizu 1995
Peak flux	1–6 keV	normal flares	1.75	Drake 1971
Radiated energy	1–6 keV	normal flares	1.44	Drake 1971
Peak flux	1.5–12 keV	GOES A2–C8 flares	1.88 ± 0.21	Feldman et al. 1997
Peak flux	3.5–5.5 keV & UV	microflares	2.18–2.23	Porter et al. 1995
Peak flux	7.7–12.5 keV	normal flares	1.84 ^a	Hudson et al. 1969 ^a
Peak flux	10–300 keV	normal flares	1.8	Datlowe et al. 1974
Peak flux	13–600 keV	HXR microflares	~ 2.0	Lin et al. 1984
Peak count rate	25–500 keV	normal flares	1.8	Dennis 1985
Peak count rate	26–500 keV	normal flares	1.54	Aschwanden & Dennis 1992 ^a
Peak count rate	>25 keV	normal flares	1.73 ± 0.01	Crosby et al. 1993
Peak flux	>25 keV	normal flares	1.59 ± 0.01	Crosby et al. 1993
Peak count rate	>25 keV	normal flares	1.7–1.9	Bai 1993
Peak flux	>30 keV	normal flares	1.8–2.2	Bromund et al. 1995
<i>Stellar:</i>				
Radiated energy, M dwarfs	0.05–2 keV	$10^{30.6} - 10^{33.2}$ erg	1.52 ± 0.08	Collura et al. 1988
Radiated energy, M dwarfs	0.05–2 keV	$10^{30.5} - 10^{34.0}$ erg	1.7 ± 0.1	Pallavicini et al. 1990
Radiated energy, RS CVn	EUV	$10^{32.9} - 10^{34.6}$ erg	1.6	Osten & Brown 1999
Radiated energy, two G dwarfs	EUV	$10^{33.5} - 10^{34.8}$ erg	2.0–2.2	Audard et al. 1999
Radiated energy, F-M dwarfs	EUV	$10^{30.6} - 10^{35.0}$ erg	1.8–2.3	Audard et al. 2000
Radiated energy, 3 M dwarfs	EUV	$10^{29.0} - 10^{33.7}$ erg	2.2–2.7	Kashyap et al. 2002
Radiated energy, AD Leo	EUV & 0.1–10 keV	$10^{31.1} - 10^{33.7}$ erg	2.0–2.5	present work

^aquoted in Crosby et al. 1993

In statistical flare studies, the identification of weak flares close to the apparently quiescent emission level becomes an ill-defined problem. Explicit detection methods discriminate against small flares due to overlap with larger flares, confusion between the many approximately simultaneous small flares, or short detection times above the significance level (Hudson et al. 1969; Audard et al. 2000). Limited signal-to-noise ratios add to the problem. Some of these complications can be overcome to some extent by fully modeling the superposition of a statistical ensemble of flares and comparing observable quantities between models and observations. An important diagnostic of this kind may be the coronal differential emission measure distribution (DEM) since it is determined by the ensemble of plasma packets heated to different temperatures. A time-integrated observation of a time-dependent heating mechanism may therefore reveal a characteristic DEM that contains diagnostics for the stochastic flare distribution (Güdel 1997; Güdel et al. 1997; the modeling described in the latter papers concentrated on small α with important effects due to large and long-lasting flares). We will derive an analytical expression for a DEM of a flare-heated corona in this paper. The present work and its companion paper (Kashyap et al. 2002) are, on the other hand, predominantly concerned with statistical light curve analysis, comparing model light curves with long monitoring observations obtained in the EUV and X-ray ranges. While Kashyap et al. (2002) focus on a detailed instrumental modeling of the *EUVE* DS instrument and a statistical analysis of the photon arrival time distribution for a sample of stars, the present paper concentrates on a dedicated, long observing campaign of AD Leonis using the *EUVE* and *BeppoSAX* satellites; two complementary methods, one presented in Kashyap et al. (2002), are applied, and the results are used to compute the emission measure distribution of a continually flaring stellar corona.

The paper is organized as follows: §3 discusses our data reduction techniques, and §4 the analysis methods. In §5 we present our results, and we discuss various features in §6. Finally, §7 presents our conclusions. Although we follow our hypothesis that all of the observed X-ray emission is due to a statistical ensemble of flares, it is convenient to use the term “quiescent” emission for the emission level at which individual flares can no longer be separated, i.e., for the quasi-steady emission.

3. DATA SELECTION AND REDUCTION

Our target for the present investigation is the nearby dMe star AD Leo. AD Leo is a well-studied flare star with a high flare rate. Its spectral class is M3 V, and its X-ray luminosity amounts to $\log L_X = 28.95$ (L_X in erg s^{-1}). We use a distance of $d = 4.90$ pc (see Audard et al. 2000 for further details on the target, and for references). Its quiescent

count rates in the *EUVE* DS, the *BeppoSAX* LECS, and the *BeppoSAX* MECS used here are, respectively, ~ 0.15 , 0.105, and 0.025 cts s^{-1} (these values refer to the mean of all flux bins in which no significant flares were evident.)

The *Extreme Ultraviolet Explorer* (*EUVE*, e.g. Malina & Bowyer 1991) data presented here were obtained in several segments between 1999 April 2 and 1999 May 15 (see Table 2). DS Remapped Archive QPOE files were rebuilt using the `euv1.8` package within IRAF. For our method 1 (see below) in which we used binned data, we applied primbsching (telemetry saturation) and deadtime corrections to all data sets, and excluded time intervals for which the combined correction factors exceeded 30%. To avoid fluctuations that may still occur within one satellite orbit window owing to residual inaccuracies in these corrections (e.g., due to the South Atlantic Anomaly), we decided to generally bin data to one bin per orbit (5663 s), which turns out to be sufficient to recognize numerous EUV flares, to resolve them in time, and to provide a good signal-to-noise ratio per bin. The light curve is shown in Figure 1. The last time interval (see Table 2) suffered from too high radiation, with correction factors higher than typically acceptable. This segment was *not* used in the subsequent analysis (for any of the methods). The final data set used for method 1 contained 470 bins.

The *BeppoSAX* satellite (Boella et al. 1997a) pointed its Low and Medium Energy Concentrator Systems (LECS and MECS, respectively; Parmar et al. 1997; Boella et al. 1997b) and its Phoswich Detector System (PDS; Frontera et al. 1997) towards AD Leo three times (Table 2), spanning a total time of 15 days for 270 ks of exposure time. Most of the observations were performed simultaneously with the *EUVE* observations. No significant signal was detected in the PDS instrument, even during flares. The three different pointings were similar, allowing us to merge the individual data sets into single LECS and MECS data sets. The cleaned and linearized event files from LECS and MECS2 (MECS2 and MECS3

Table 2. OBSERVING LOG (1999 APRIL/MAY)

Segment	Instrument	from UT MM/DD hh:mm	to UT MM/DD hh:mm	HJD range -2440000.5
I	<i>EUVE</i>	04/02 16:09	04/04 04:54	11270.673–11272.204
II	<i>EUVE</i>	04/05 00:46	04/14 16:41	11273.032–11282.695
III	<i>EUVE</i>	04/17 03:32	04/24 09:27	11285.147–11292.394
IV	<i>EUVE</i>	04/25 16:29	05/04 11:41	11293.687–11302.487
V	<i>EUVE</i>	05/06 16:41	05/16 05:11	11304.695–11314.216
I	<i>BeppoSAX</i>	05/01 06:34	05/03 04:48	11299.274–11301.200
II	<i>BeppoSAX</i>	05/08 05:47	05/10 13:10	11306.241–11308.549
III	<i>BeppoSAX</i>	05/12 08:39	05/15 15:05	11310.360–11313.628

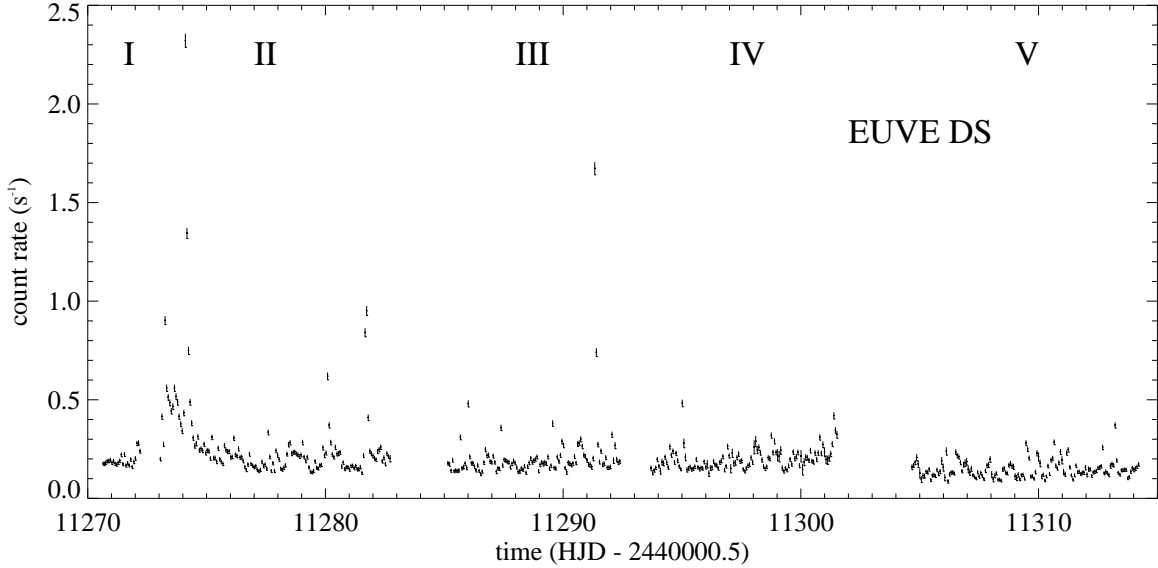


Fig. 1.— *EUVE* DS light curve of AD Leo (before primbsching and dead time corrections), obtained between April 2, 1999, and May 16, 1999. Segment V suffers from “dead spot” reduction in effective area and from high radiation. The 1σ error bars are typically ± 0.01 ct s $^{-1}$ and have been plotted.

combined file) from the SAX Science Data Center pipeline processing were filtered with the good time intervals that exclude the events occurring while there was no attitude solution. Because of the overall faster variability seen in the X-ray range and in order to maximize the number of available points while still retaining a sufficient signal-to-noise ratio to detect a large number of flares, we decided to resolve each orbit visibility interval into a few bins of length 200 s (a test performed with 1 bin per orbit provided compatible results that were, given the small number of points, ill-constrained). We thus used a total of 658 bins for the LECS light curve and 1363 bins for the MECS light curve. The MECS has more bins since it observed longer (up to about 3000 s) during each orbit, and it suffered from fewer bad time intervals during the on-source observations. The light curves of all three segments are shown in Figure 2.

Average quiescent spectra were extracted for LECS and MECS, excluding obvious large flares (but still including small flares because, in our working hypothesis, there is no strict difference between flaring and non-flaring emission). The source was extracted inside circular regions of radius 8.17' and 4' for LECS and MECS, respectively. Blank sky pointings were used to model the instrumental and sky X-ray backgrounds. We checked the local background with two semi-annular regions for LECS (see Parmar et al. 1999 for full details) and two

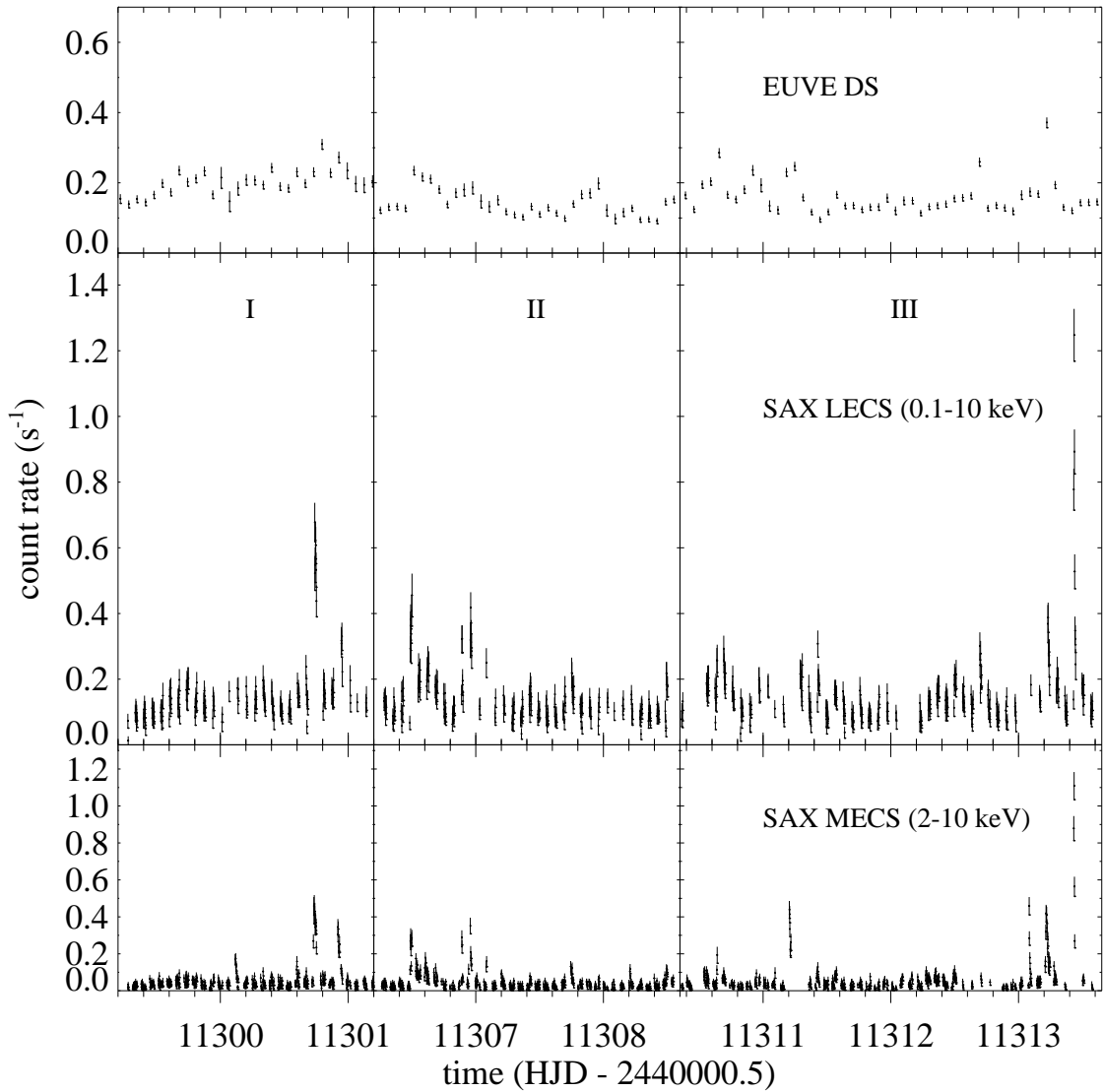


Fig. 2.— *BeppoSAX* MECS and LECS light curves, compared with simultaneous *EUVE* DS data. Roman numerals refer to the *BeppoSAX* intervals (see Table 2). Note that *EUVE* DS data obtained during *BeppoSAX* intervals II and III are unreliable due to high radiation background and were not used.

regions perpendicular to the on-board calibration sources for MECS. We found that the blank-sky backgrounds are suitable for our data. We used the `lemat` tool in SAXDAS 2.0.1 to create LECS response matrices, and we adopted the standard MECS responses distributed by the mission (September 1997). Finally, the data were grouped with a minimum of 25 counts per bin. Data from 0.12 to 4 keV were kept for the LECS spectrum, while data from 1.65 to 10.5 keV were kept for the MECS23 spectrum (see Fiore, Guainazzi, & Grandi 1999). We fitted the combined spectra in XSPEC (Arnaud 1996) using several isothermal collisionally ionized equilibrium plasmas (the so-called MEKAL code) with a fixed interstellar hydrogen absorption column density $N_{\text{H}} = 10^{18} \text{ cm}^{-2}$ (Sciortino et al. 1999). We also introduced a free constant factor to the LECS spectrum to account for cross-calibration discrepancies in the overall effective areas. We left the Fe abundance free while we kept the other abundances at solar photospheric values. A three-temperature model provided a reasonable fit (Table 3). Finally, we derived an emission measure distribution (DEM) from the combined LECS and MECS data in SPEX, averaging the DEMs from the polynomial and the regularization methods as described in Kaastra et al. (1996a) (this is further discussed in § 6.4).

4. ANALYSIS

We analyzed the calibrated and cleaned data using two different methods. Since the present data quality does not allow us to model the run of temperatures and emission measures of individual flares (and therefore to integrate the *modeled* radiative losses across complete flares), we will assume that the observed count rate is proportional to the total X-ray flux from the star. We will discuss the reliability of this assumption in §6.3.

Table 3. FIT TO THE QUIESCENT *BeppoSAX* DATA

$\log N_{\text{H}}^{\text{a}}$ (cm^{-2})	kT_1 (keV)	kT_2 (keV)	kT_3 (keV)	$EM_1/10^{50}$ (cm^{-3})	$EM_2/10^{50}$ (cm^{-3})	$EM_3/10^{50}$ (cm^{-3})	Fe ^b	f ^c	χ^2/dof
= 18.0	0.18 ± 0.01	0.68 ± 0.01	1.80 ± 0.08	5.4 ± 0.4	13.6 ± 0.4	4.5 ± 0.2	0.54 ± 0.03	0.69 ± 0.03	315.48/261

^aFixed value

^bAbundance relative to the solar photospheric value (using values from Anders & Grevesse 1989)

^cEffective-area cross-calibration factor LECS/MECS23

4.1. Count Rate Distributions

We compare the count rate distributions of the light curves with simulated data sets composed of a statistical flare distribution. The simulations are performed as follows: We first calculate a statistical power-law distribution of flare energies (equation 1) specified by three free parameters: the total number of flares during the simulation time (flare rate R_f), the power-law index α , and a lower cut-off energy E_0 . The latter is necessary for practical reasons but must also physically exist in the case of $\alpha \geq 2$. The count rate normalization is arbitrary and will be re-normalized later. The flares, initially defined as delta functions, are randomly distributed in time. The length of the simulation time interval was chosen to contain 5490 bins, i.e., about ten times more than the binned *EUVE* and *BeppoSAX*/LECS light curves and about 4 times more than the MECS light curve, i.e., we compare the observation with about ten (resp. four) statistical realizations of a simulation of equal length.

This model light curve is then convolved with a calculated exponential decay profile with pre-set decay time constant τ . This latter form is typical of that commonly observed for stellar flares. The model flares start at their peaks (i.e., the rise phase of the flare is very short, compatible with the observations). We note that the individual flare decay times vary somewhat, also due to superimposed flares that may widen the apparent flare profile. Experiments with a profile that was half as wide for the LECS and the MECS data showed, however, that the results are quite insensitive to the precise profile shape. The flare decays are generally considerably slower in the EUV range than in soft X-rays. Based on a detailed analysis with fully resolved *EUVE* DS data sets including ours, a decay constant of 3000 s proves appropriate (Kashyap et al. 2002), and we adopt this value for consistency with the study presented by the latter authors although we will test (as they did) variable decay times as well. Most rapid features in the LECS and MECS required a characteristic decay time scale of only 300–400 s; we adopted a decay time of 360 s.

Since during a considerable fraction of the satellite orbit the target star is not accessible, we also simulated the effects of “windowing”. The DS instrument observed AD Leo contiguously for typically 1520 s during *EUVE*’s 5663 s orbit, the LECS for 1400 s and the MECS for 3000 s during the 5780 s *BeppoSAX* orbit. One anticipates that correcting for this effect is statistically of little importance. In particular, since the flare decays are nearly exponential, a flare from which the initial part is cut off behaves like a flare detected at peak time, with the same decay time scale but with a smaller amplitude. In this case, flares of a given energy statistically shift to somewhat lower energies. Since the flare decay constants are similar or equal for all flares, their count rates are statistically suppressed by the same factor, resulting only in a lower normalization of the count rate distribution, which

is irrelevant. Our conjecture was verified with appropriate models that cut simulated flares arbitrarily the same way as the real observation does.

We then sort all bins of the light curve, both for the observed and the model light curve, in order of increasing count rate c to obtain a cumulative count rate distribution $\mathcal{N}(< c)$ (number of bins with a count rate up to a given c , where we normalize \mathcal{N} by the total number of bins, i.e., $0 \leq \mathcal{N} \leq 1$; see Fig. 3–6). The cumulative distribution is very sensitive to systematic deviations in the shape of the count rate distribution as produced, for example, by different flare energy distributions. Since the observed and the model distributions are not mutually normalized in their count rates, we renormalize the (cumulative) model distribution such that the average count rate within a range $[\mathcal{N}_1, \mathcal{N}_2]$ is the same as the average count rate in the corresponding \mathcal{N} range of the observed distribution. At this stage, noise corresponding to the observed Poisson noise is added to the model points, and the model data points are sorted again in count rate.

The low end of the count rate distribution is inherently ill-defined. It is sensitive to statistical fluctuations from the superposition of numerous weak flares while at the same time the relative errors are largest in that range. Further, tails from a few long-decay flares may modulate this count rate level in time. Also, intrinsic non-flaring variability such as due to emerging magnetic loops or rotational modulation can introduce slow variations. We therefore keep the final normalization interval above zero, namely at $[\mathcal{N}_1, \mathcal{N}_2] = [0.1, 0.5]$, and do not further consider the portion at $\mathcal{N} < 0.2$ (< 0.1 for LECS/MECS).

For any selected α , we generated a large family of models that differ only in their flare rates. We selected the example that minimizes the largest vertical distance between the model and the observed cumulative distributions (i.e., minimal $\max(|\mathcal{N}_{\text{obs}} - \mathcal{N}_{\text{model}}|)$) as our best fit. The traditional Kolmogorov-Smirnov test cannot be applied to the two distributions since the normalization (one of the required fit parameters) has been derived from the properties of the distributions themselves. We rather *simulate* a sample of observations with defined properties (α , R_f , and E_0) and a length equal to the real observation. We then analyze each simulated observation precisely the same way as the real observation in order to find statistical approximations to the confidence limits of our results. If the model distribution is too shallow (α too small) we find an excess of large count rates, i.e., the model cumulative distribution lies below the observed cumulative distribution toward larger count rates (see Fig. 3–6 below). Conversely, if the model distribution is too steep (α too large), then the model distribution lies above the observed distribution.

4.2. Analysis of Photon Arrival Time Differences

Kashyap et al. (2002) present a detailed description of the second method that is founded on a detailed modeling of the *EUVE* DS detector. We provide only a brief summary. The basis of the method is that, as count rates rise and fall with flaring activity, the intervals between photon arrival times decrease and increase according to the Poisson distribution appropriate for the count rate at any given moment. These changes in the arrival time differences (δt) cast a signature on the photon event list that changes according to the nature of the underlying source variability. Thus, for a given observation, the observed distribution $f(\delta t)$ summarizes the character of the variability of the source during that observation. A fixed flare distribution (equation 1) gives rise to a definite $f(\delta t)$ provided that the observation is of sufficient duration to contain a representative range of intensities, and different flare distributions will give rise to different arrival-time difference distributions. Note that $f(\delta t)$ is not sensitive to the actual temporal locations of the flares, but rather depends only on the stochastic ensemble described by equation 1. The power-law index, α , that best describes the observed light curve is determined by comparing the observed arrival time difference distribution $f_{obs}(\delta t)$, with simulated distributions $f_{sim}(\delta t)$.

This method was developed to deal easily and rigorously with the windowing inherent in low Earth orbit observations (with a typical observing time of 30 minutes for each ~ 90 minute orbit), such as those obtained by *EUVE*, and to allow for proper treatment of telemetry saturation (“primbsching”) and deadtime effects that can introduce somewhat variable corrections during one orbit. Since we deal here with photon lists, a proper treatment of the corrections *continuously in time* is important. The advantage of the method is that it operates directly on the observed photon event list, avoiding the need for time binning. Simulated event lists can be windowed in exactly the same way as the observed event list, and primbsching effects can be applied to the simulated events, censoring them in the same stochastic way as the observed events.

We assume here that the observed light curves can be described by the sum of a flaring component, with a power-law frequency distribution of flare energies as described by equation 1, and a constant component. The flaring and constant components are described by the *flare rate* C_f , and a “quiescent background” rate C_b , respectively. As for the first method, the flares are assumed to be impulsive events whose count rates decay exponentially with a time scale of a few thousand seconds. The exact decay time can be varied to best match any observed flares or the observed and synthetic photon event lists themselves. In practice, we have found that results obtained for decay times in the range 1000–5000 s are typically very similar because the extensive overlapping of flare events tends to decrease the sensitivity of the results to this parameter (Kashyap et al. 2002); the final results presented here assume

a decay time of 3000 s, identical to the value found and applied by Kashyap et al. (2002). For specified values of C_f and C_b , a synthetic light curve corresponding to the entire interval covered by the observed light curve can then be realized through a Monte Carlo algorithm, assuming a random distribution of flares in time but subject to the power-law frequency distribution of total energies. This light curve is then windowed by the observed photon event “good time intervals” and a synthetic event list is derived through a Poisson realization of the resulting light curve. The synthetic event list is then pruned by discarding photons at a rate corresponding to the observed Primsch factor. The remaining set is identical in its “instrumental characteristics” to the observed data and the observed and synthetic event lists can be compared directly.

Observed photon arrival time differences are compared to those synthesized across a grid of the parameters α , C_f and C_b using the χ^2 statistic to compare $f_{sim}(\delta t)$ with $f_{obs}(\delta t)$. A number of simulations (typically ~ 10) are carried out and the median value among the resulting χ^2 are used to compute the likelihood of obtaining the observed data for the given set of parameters $\{\alpha, C_f, C_b\}$. In the case of AD Leo, we have examined each of the three *EUVE* observation segments II, III, and IV independently (Table 2), treating them as three different observations, as well as treating the whole sequence II-IV at once. This enabled us to examine the degree of consistency of our derivation of α from segment to segment.

5. RESULTS

5.1. Parameters and Tests

Our simulated light curves were generated assuming an exponential flare decay time τ independent of the flare energy or amplitude. If the decay time increases systematically with the total radiated energy, e.g., $\tau \propto E^\beta$, then the flare amplitudes increase less than proportionally with the energies, which may be interpreted as a steeper energy distribution. However, increasing the decay time of larger flares produces more bins at large count rates (but only an equal number of additional bins at low count rates), and this effect counteracts the apparent steepening of the energy distribution.

Observationally, a dependence of the decay time on energy is marginal. Aschwanden et al. (2000) investigated scaling laws from solar nanoflares to larger flares, covering 9 orders of magnitude in energy. While most of the geometric and physical parameters exhibit a strong scaling with the flare size, Aschwanden et al. report that the time scale (radiative or conductive) does *not* depend on the flare size. In fact, as stronger flares tend to show larger electron densities and higher coronal peak temperatures (§3.1 in Aschwanden et al. 2000),

they should radiatively or conductively decay faster than small flares, which is not observed. The range of decay times (their Table 2) is much larger than any possible trend between nanoflares and large flares. Feldman et al. (1997) measured soft X-ray FWHM durations of a large sample of flares over three orders of magnitude and found no trend. The differences between flare decays are due to scatter within classes of flares of about equal energy. Shimizu (1995) investigated energies and durations of small solar active-region transients and again found no clear trend in the durations over four orders of magnitude in peak count rate. We inspected the best defined flares in our data although superpositions of flare profiles may introduce ambiguity. The MECS data are best suited for such an analysis since they provide the longest intervals of visibility per orbit, a high flare-to-quiescent emission contrast, and a time bin resolution of 200 s. We found no trend for a correlation between flare amplitude and decay time; the scatter in the decay time itself dominates. The same holds true for the other data sets. However, the sample of selected large X-ray flares of Pallavicini et al. (1990) from *different* stars shows a weak trend if four orders of magnitude in radiated energy are included, but the total variation is no larger than the scatter in duration at a given energy. For individual stars, there is no clear trend. Their data sample can be best fitted with a relation $\tau \propto E^{0.25}$. Given that our dynamic range (ratio between largest to smallest explicitly detected flare count rate) is of the order of 10–20 for binned data, this effect may statistically influence the results. We therefore tested the DS, LECS, and MECS analysis by introducing variable decay times as specified above.

We have used two realizations of our analysis for the binned *EUVE* data (method 1) that show a well-developed quiescent emission. First, we applied it to the data from which the (constant) quiescent level was subtracted. In this case, we test whether we can find a model distribution that is compatible with the *observed* flare emission. Second, we applied the method to the complete data including the quiescent emission. Since the latter, in our model, should be the superposition of unresolved small flares, the addition of a quiescent level simply corresponds to the extrapolation of the power law to lower energies, and we expect that the power-law index does not significantly change. This second realization also allows us to derive the lower cut-off energy E_0 required to explain the quiescent emission. The comparison between the two realizations could potentially reveal a basic difference between quiescent and flaring emission. If the flare energy distribution does not steadily continue toward more numerous small flares that eventually merge with the quiescent level, then the first realization would be subject to a cut-off energy possibly above the quiescent level (bimodal flux distribution), and the derived values for α may differ. These two extreme cases will further be discussed below. The contrast between flares and the quiescent emission is much larger in the *BeppoSAX* data; we treated only the complete data sets in these cases for the primary results but also subtracted the quiescent level for an assessment of the confidence

ranges (see below).

5.2. Basic Findings

We first discuss results obtained using method 1 under the assumption of constant exponential decay times τ for all flares. Figure 3 shows results for the *EUVE* light curve of AD Leo (segments I–IV) from our first method. The top figure represents the light curve binned to one point per orbit (5663 s). Here, a constant quiescent count rate of 0.13 ct s^{-1} has been subtracted, corresponding to the lower envelope of the light curve. The x-axis (“time”) gives the sequential bin number, with observing gaps at 30, 200, and 340 fully considered. The alternative analysis in which the initial large flare was excluded used only bins above bin no. 70.

The three lower rows then illustrate, in this order, the best fit found in the analysis (i.e., optimum α and optimum flare rate), a selected case with too low α (but again optimum flare rate), and similarly a case with too high α . In each case, the figure on the left shows an extract of the simulated and normalized light curve with noise added, while the figure on the right shows the respective cumulative distributions. In the latter, the solid line shows the observed cumulative count rate distribution $\mathcal{N}(< c)$ while the dashed line illustrates the normalized count rate distribution from the model. The two dotted vertical lines indicate the range used to normalize the model distribution to the observation. Our statistical fit criterion (minimizing the largest vertical distance between the two distributions) was applied only above the dashed horizontal line (above $\mathcal{N} = 0.2$ or 0.1). The dotted function close to and around the horizontal $\mathcal{N} = 0$ line illustrates the difference “model – observation” for the cumulative distributions. Evidently, the optimum index is $\alpha \approx 2.2$ in this case, while values as low as 1.9 or as high as 2.7 are considerably worse.

Figure 4 shows the equivalent analysis but without subtraction of a quiescent level. The optimum value is formally found at $\alpha = 2.1$ although the cumulative count rate histogram suggests a somewhat higher α . The fit is generally somewhat poor, but a test in which the quiescent level was reduced by 50% still produced $\alpha = 2.1$. Lastly, Figures 5 and 6 show the results from the analysis of the LECS and MECS light curves, respectively. Only the observed light curve, an extract of the optimum model, and the cumulative distributions are shown. We find optimum values of $\alpha = 2.4$ and 2.2, respectively.

The statistical confidence ranges derived from our sample of simulated observations are as follows. Approximately 90% of best-fit solutions for the *EUVE* DS simulations (performed for $\alpha = 2.0$ and $\alpha = 2.2$) were found symmetrically within a range of ± 0.1 centered at the

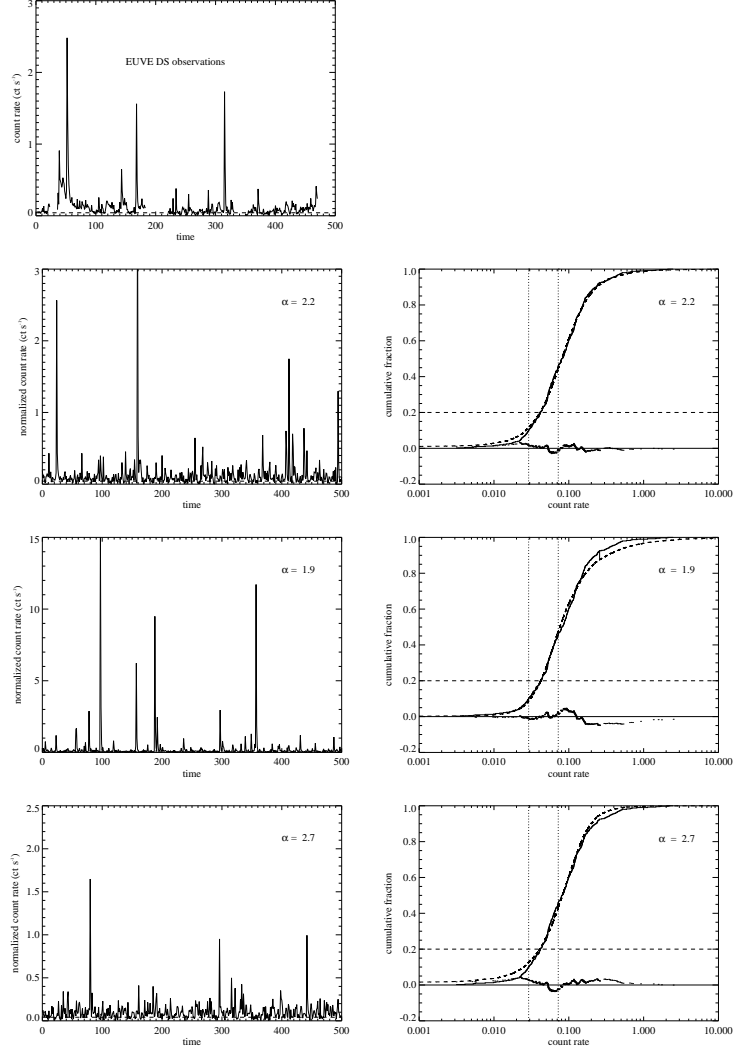


Fig. 3.— Examples of statistical flare simulations from method 1 for different power-law distributions. The *EUVE* DS data set of AD Leo is shown. Only emission exceeding quiescent level has been modeled. The early large flare is included. Three simulated best-fit examples for different α are shown. **Top figure:** Observed light curve. **Second line:** Optimum case; $\alpha = 2.2$. **Third line:** Too shallow distribution with $\alpha = 1.9$. **Bottom line:** Too steep distribution with $\alpha = 2.7$. For 2nd, 3rd, and bottom figure panel: **Left:** Simulated light curve (extract, normalized). Dashed line marks the lower limit to count rates that were considered for optimizing the fit. **Right:** Cumulative count distribution for data (solid) and model (dashed), and difference (dotted, around zero line). The maximum difference (vertical bar between observation and model) is minimal for the best fit. The two vertical dotted lines mark the interval for the model count rate normalization. The horizontal dashed line marks the count rate level above which the differences between observation and model were considered.

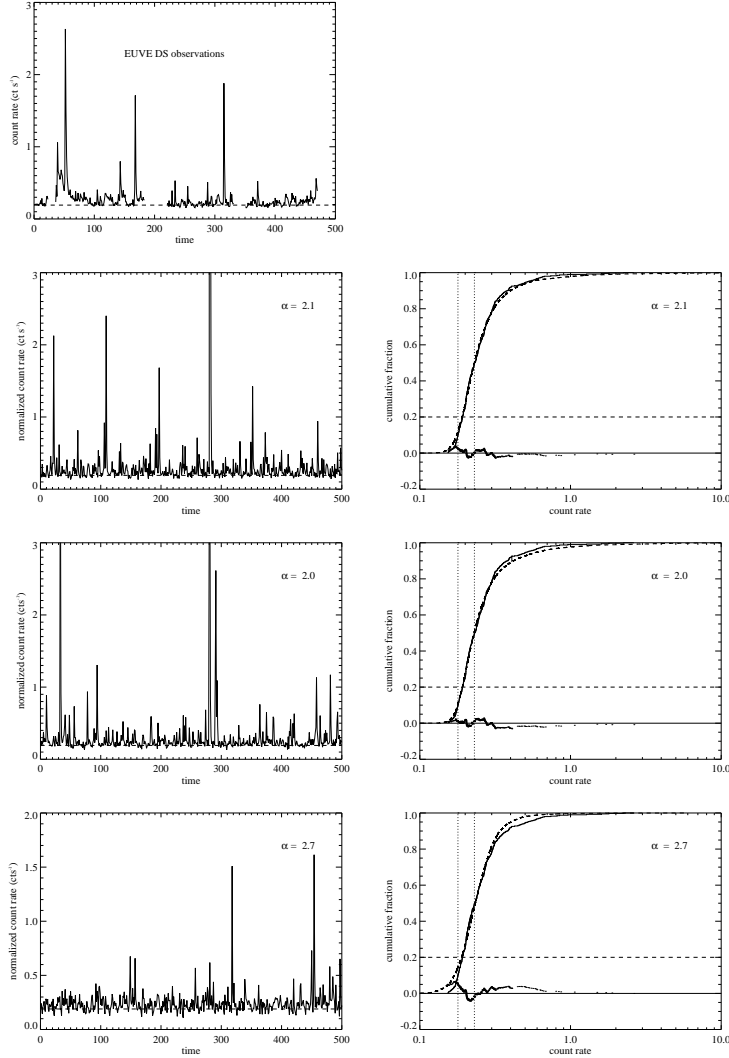


Fig. 4.— Similar to Fig. 3 (method 1), but all emission, including quiescent emission, has been modeled. **Top panel:** Observed light curve. **Second panel:** Optimum case; $\alpha = 2.1$. **Third panel:** Too shallow distribution with $\alpha = 2.0$. **Bottom panel:** Too steep distribution with $\alpha = 2.7$.

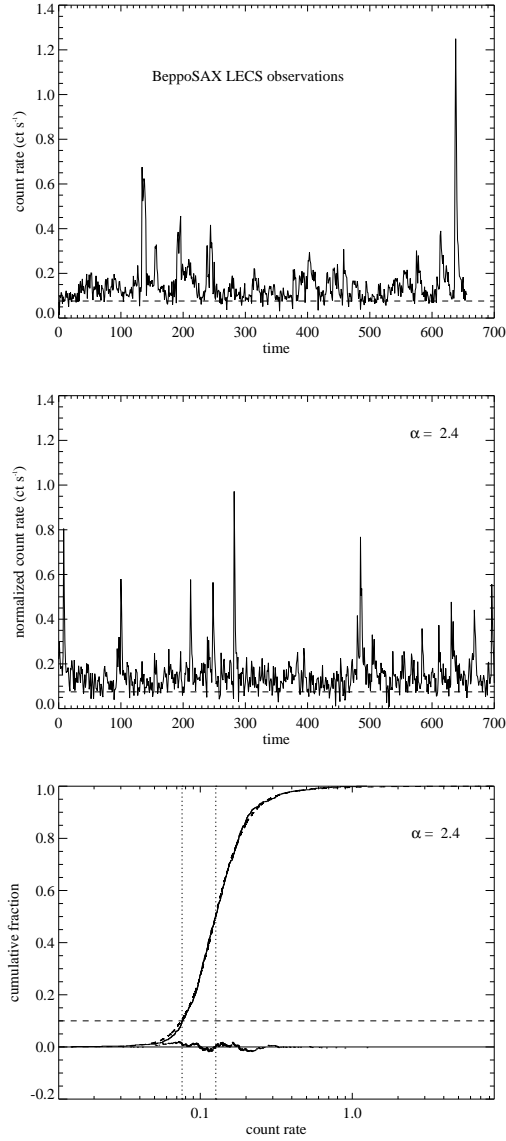


Fig. 5.— Similar to Fig. 3 (method 1), for LECS. Only optimum model is shown, with $\alpha = 2.4$. Gaps between observation segments and between orbits are not retained.

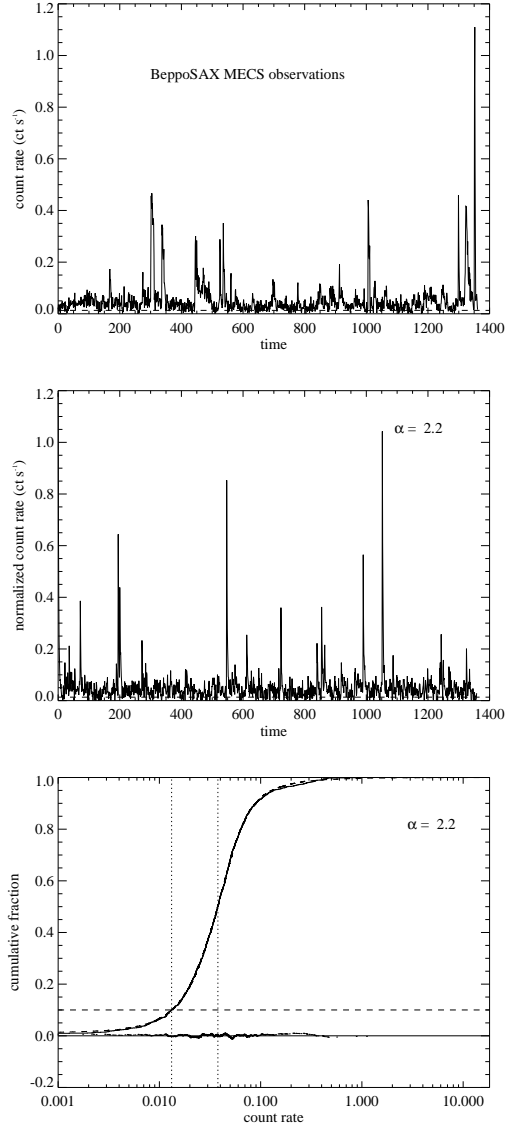


Fig. 6.— Similar to Fig. 3 (method 1), for MECS. Only optimum model is shown, with $\alpha = 2.2$. Gaps between observation segments and between orbits are not retained.

correct α . We thus adopt $\Delta\alpha = \pm 0.1$ as our 90% confidence limits for the *EUVE* DS results. The lower signal-to-noise ratio of the *BeppoSAX* data constrained the simulation results less well, probably due to the large dominance of the noise fluctuations at low count rates. We therefore repeated the analysis (both for the real and the simulated observations) constructing cumulative distributions from those data only that exceed the quiescent level by 1σ , thus selecting predominantly the visible flares only. For the LECS, $\alpha = 2.4$ was confirmed, while for the MECS, we found optimum fits for $\alpha = 2.0$. From the sample of simulated observations, we again find a 90% width of about ± 0.1 , although α is slightly underestimated by 0.1 on average. This effect is probably due to selectively choosing the larger count rate bins. We conservatively adopt a combined (statistical and systematic) uncertainty of ± 0.2 for the LECS and MECS (90%).

The following systematics are evident (Table 4): (i) In all cases, we find acceptable values for α at or above 2, with $\alpha = (2.1 - 2.3) \pm 0.1$ for the DS data, $\alpha = 2.4 \pm 0.2$ for LECS and $\alpha = (2.0 - 2.2) \pm 0.2$ for MECS. When we excluded the large flare in the DS light curve, the distribution steepened by $\Delta\alpha \approx 0.1$ (Table 4), an effect that is to be understood as follows: The presence of a large flare will tend to give a smaller α because comparatively less power will be contained in smaller flare events. Conversely, the selective elimination of the population of the strongest flares steepens the distribution although a genuine single power law cannot be retained if too large a fraction of the distribution is eliminated. The long decay of the large flare clearly also biases the count rate distribution toward a lower α (adding a large number of bins at high count rate levels). Overall, thus, the DS and the LECS ranges for α agree. The MECS range appears to be systematically lower. We will discuss this effect further in Section 6.3.

The results from the second method, based on photon arrival statistics, are illustrated in Figures 7a–7d, where the derived probabilities of power law indices α matching the observed index are plotted as a function of α . The results are also summarized in Table 5. The first three figures illustrate the derived probabilities for the three segments II, III, and IV treated separately, while the fourth shows the results of the analysis of the whole data set II-IV treated as a single observation. The important feature of all these figures is that the most probable value of α is again always greater than 2 but less than 2.3, based on 90% or 95% confidence intervals. Segment II appears to have an optimum index that is slightly lower than that of the last two segments. This is caused by the large flare, which contains a significant fraction of the total observed counts in that segment (see above). The confidence intervals for the last two segments are remarkably similar, indicating $2.1 \leq \alpha \leq 2.3$. The most probable value of α based on all three segments (Figure 7d) is $\alpha = 2.2$. The values found here are thus in excellent agreement with results from the first method.

Table 4. α VALUES FOR AD LEO FROM METHOD 1; MINIMUM MODEL FLARE ENERGIES AND LUMINOSITIES^a

Data set, segment	bin size (s)	α (90% error)	Minimum flare counts	Minimum flare energy (erg)	Minimum peak luminosity (erg s^{-1})	Detection limit flare energy (erg)	Detection limit peak luminosity (erg s^{-1})
DS I–IV ^b	5663	2.2(0.1)	62	1.7×10^{31}	5.8×10^{27}	3×10^{31}	1×10^{28}
DS I–IV ^c	5663	2.3(0.1)	60	1.7×10^{31}	5.5×10^{27}	3×10^{31}	1×10^{28}
DS I–IV ^d	5663	2.1(0.1)	0.5	1.4×10^{29}	4.8×10^{25}	3×10^{31}	1×10^{28}
DS I–IV ^e	5663	2.3(0.1)	3.5	9.6×10^{29}	3.2×10^{26}	3×10^{31}	1×10^{28}
LECS I–III	200	2.4(0.2)	0.8	3.8×10^{29}	1.0×10^{27}	1.4×10^{31}	4×10^{28}
MECS I–III	200	2.0–2.2(0.2)	0.4	1.1×10^{30}	2.9×10^{27}	3.6×10^{31}	1×10^{29}

^aFor given time bin size and for the optimum case; minimum flare counts/energy/peak luminosity refer to smallest flares used in the simulation with optimum KS test result. Detection limit refers to 3σ levels for the respective bin size.

^bquiescent level subtracted, all data

^cquiescent level subtracted, large flare excluded

^dquiescent level included, all data included

^equiescent level included, large flare excluded

Table 5. α VALUES FOR AD LEO FROM METHOD 2 (DS)

Segment DS	Most probable α	95% Confidence Interval
II	2.07	2.00–2.13
III	2.22	2.11–2.31
IV	2.25	2.13–2.30
II–IV	2.19	2.14–2.23

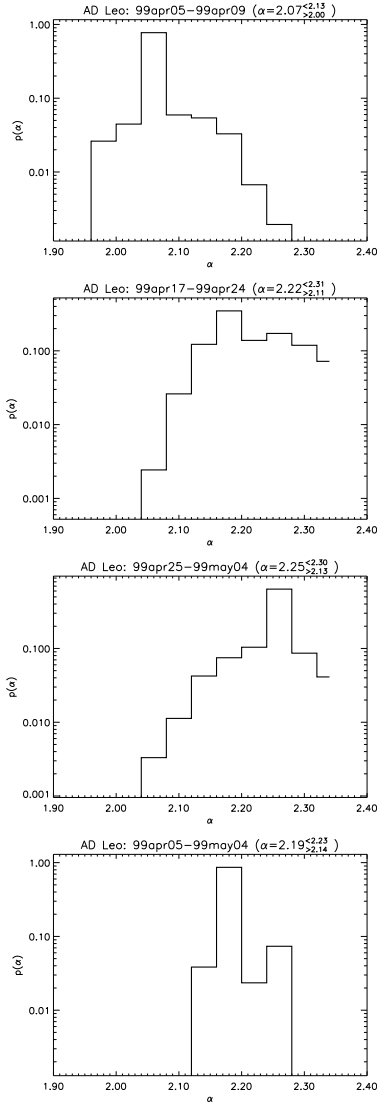


Fig. 7.— The derived probability of the power-law index α matching that of the *EUVE* DS observations of AD Leo based on the distributions of photon arrival time differences (method 2). The most probable value of α corresponds to the peak value of each distribution and is printed together with the corresponding 95% confidence intervals at the top of each figure. From top to bottom: **a)** Segment II, including the large flare. **b)** Segment III. **c)** Segment IV. **d)** Segments II-IV combined.

We further investigated the case for an exponential decay time $\tau \propto E^\beta = E^{0.25}$. In the first method, sufficiently small flares will have decay times much smaller than the bin length and thus the method is sensitive only to their total energy contribution, but not to their decay time. Given our relatively coarse binning, we thus expect to find rather stable results for α . This is confirmed, with deviations of no more than ± 0.1 in α . The second method is much more sensitive to details in the light curve and could, in principle, find both power-law indices β and α . In practise, however, there is an acceptable family of solutions (α, β) . The acceptable α increases with increasing β , reaching values up to 2.6–2.8 for $\beta = 0.25$. We interpret this as being due to a larger time occupation by relatively large count rates, i.e., short photon arrival time differences, if the energetic flares are stretched in time relative to the small flares (despite the corresponding decrease in peak count rate). The model light curve thus appears to be “too hard”, and a higher α is required to match the statistics of the observation. If we require agreement with method 1, then $\beta = 0$ and $\alpha = 2.2$, compatible with the absence of a detectable trend in the decay times. Even without constraining method 2, the lowest possible α range (for the lowest acceptable $\beta = 0$) is around 2.2, i.e., values below 2 remain excluded.

6. DISCUSSION

6.1. The Validity of Power Laws

The present analysis was primarily motivated by the finding that the occurrence frequencies of solar flare energies are distributed in power laws. Although some statistical models support such distributions (e.g., Lu & Hamilton 1991; Vlahos et al. 1995) their physical cause is a matter of debate. Indeed, there is little reason to assume that the same power laws strictly hold for all classes of flares and for all coronal regions (active regions, magnetic areas above the network, quiet regions, etc). A simple estimate, for example, suggests the presence of a high-energy cut-off: An average coronal magnetic field of strength 100 G in a half-spherical active region of radius 10^{10} cm contains 8×10^{32} erg of magnetic energy. Stronger flares (as often observed in active stars) either require stronger magnetic fields or a larger volume, but both are constrained by the maximum magnetic field strength available in the photosphere and, respectively, by the volume of active regions (that are related to the size of bipolar magnetic regions in the photosphere and by about two coronal scale heights; Serio et al. 1981). A high-energy cut-off is also suggested from avalanche model simulations (Lu & Hamilton 1991; Lu et al. 1993) and evidence for its existence has been found in observations of small solar active regions (Kucera et al. 1997), and in investigations of time-dependent α values for solar flares (Bai 1993; Bromund, McTiernan, & Kane 1995).

On the low-energy side, the power-law index may change due to physical changes in the energy release (Hudson 1991) and this seems to be the case for solar microflares as opposed to the larger flares (Krucker & Benz 1998). A low-energy cut-off is also required to confine the total radiated power if $\alpha \geq 2$ (see §1).

We do not construct the flare distributions explicitly with our methods, but use model light curves for statistical comparison. It is, however, clear that single power laws describe the observed light curves acceptably well. Although flare energies detected by these observations are comparable to medium-to-large solar coronal flares, we find α values that are markedly larger than those reported for equivalent solar flares, but that resemble those recently reported for solar microflares with $\approx 10^6$ times smaller energies. Typical activity indicators for active stars such as ours (like L_X/L_{bol} , or the surface X-ray flux) are of order 1000 times larger than the Sun’s. It thus appears that the regime of steep power-law indices ($\alpha > 2$) is shifted upwards in energy on active stars, and that we see an equivalent population of flares at larger energies. We find power-law indices around 2.0–2.5 and our methods exclude values below $\alpha = 2$ for the softer DS and LECS light curves. Furthermore, the smallest flare energies that we require to fully model the observations lie considerably below the flare detection limit in the binned light curves (Table 4) although our second method may reach a sensitivity close to such values (Kashyap et al. 2002). Like the solar microflares, our population of flares may thus be sufficient to energize the complete corona, including the quiescent emission, if the power-law is extrapolated to flares with radiated energies of a few times 10^{29} erg (Table 4). Such energies correspond to relatively moderate flares in the solar context. These conclusions fully support the findings by Audard et al. (1999, 2000).

6.2. The Minimum Flare Energies and Quiescent Emission

A lower cut-off to the flare energies is required if $\alpha \geq 2$. The cut-off does not imply that lower-energetic flares do not exist. But it implies that their occurrence rate cannot follow the extrapolation of the power-law found at higher energies but must be considerably smaller, effectively introducing a cut-off below which flares contribute little. Our simulated model light curves were calculated assuming such an energy cut-off. We determined the cut-off energy after renormalization and thus found the minimum number of counts of any of the simulated flares. The values are reported in Table 4, column 4. To convert the total number of counts to total (radiated) flare energy, we computed the count-to-energy conversion factor as follows: A 3-temperature model (reported in Table 3) determined from the LECS and MECS data by spectral fitting of the quiescent emission was convolved with the response matrices of each of the three instruments. We thus obtained the expected total count rates

in the detectors, and by integrating the complete spectrum from 0.01 keV to 50 keV we computed the total coronal luminosity. We thus find that one detected (quiescent) count corresponds to 2.8×10^{29} erg for the *EUVE* DS, to 4.8×10^{29} erg for the *BeppoSAX* LECS, and to 2.6×10^{30} erg for the MECS. From this, we obtain the minimum energy of flares used for the simulation, as shown in column 5 of Table 4. In other words, extrapolating the power-law distribution of flares down to the reported energies is necessary and sufficient to explain the complete observed quiescent flux. The LECS provides a lower limit of 4×10^{29} erg. For the derived flare time profile, this energy corresponds to a peak luminosity of approximately 1×10^{27} erg s⁻¹ in the combined X-ray and EUV ranges. Such flares correspond to small solar flares. Similar values hold for the MECS and DS data (Table 4, columns 5 and 6).

We note that the actually *detected* flares in the binned light curves (method 1) typically exceed these levels by ~ 2 orders of magnitude. A small flare reaching a peak count rate 3σ above its pre-flare level corresponds to 3×10^{31} erg in the DS, 1.4×10^{31} erg in the LECS, and 3.6×10^{31} erg in the MECS (Table 4, column 7). The apparently quiescent level is thus composed of flares between the cut-off limit and the 3σ count rate detection limits. In terms of peak luminosity, this interval covers the $\sim 5 \times 10^{25} - 10^{29}$ erg s⁻¹ range (see Table 4, columns 6 and 8, for details). Assuming an average radiative loss function (radiative energy loss per unit EM) of $\Lambda = 2 \times 10^{-23}$ erg cm³ s⁻¹ (appropriate for $T = 5 - 40$ MK) we find that the peak EMs of these flares are approximately $2.4 \times 10^{48} - 5 \times 10^{50}$ cm⁻³ for the DS quiescent level, $5 \times 10^{49} - 2 \times 10^{51}$ cm⁻³ for the LECS quiescent level, and $1.5 \times 10^{50} - 5 \times 10^{51}$ cm⁻³ for the MECS quiescent level. From Figure 2 of Feldman et al. (1995) we estimate that the peak temperatures of these flares are 15–30 MK for the DS, 25–33 MK for the LECS, and 27–37 MK for the MECS (after Aschwanden 1999, these temperatures are smaller by a factor of ~ 1.5). If we consider that most of the flares in the power-law distribution are close to the lower end of the temperature intervals, we see that the LECS quiescent level is primarily composed of flares that reach no more than about 20 MK at peak but mostly reside at lower temperatures. The MECS effective area shows a steep gradient below 25–30 MK, thus most of the LECS quiescent emission is suppressed in the MECS. The 3-T fit explicitly shows that the bulk quiescent plasma is at temperatures around 10 MK (Table 3).

The two *BeppoSAX* light curves indeed look qualitatively different (Fig. 2). Although the same flares are present in both light curves, the LECS shows appreciable quiescent emission while the MECS does not. The contrast between strong flares and low-level emission is much stronger in the latter. This difference is a consequence of different temperature sensitivities of the detectors, the MECS being insensitive to low-level emission from presumably cooler plasma. To quantify this hardening effect, the count rates were first normalized to the average quiescent count rate level. Fig. 8 (left) illustrates the relation between LECS and simultaneous MECS count rates for 658 bins of 200 s each (see Fig. 2) along the complete

BeppoSAX light curve. It shows a pronounced deviation from proportionality: the harder MECS emission increases faster than the corresponding softer LECS emission, i.e., the emission hardens with increasing overall count rate. The best-fit power-law in this figure has an index of 1.45 ± 0.02 .

We thus find a natural explanation for the largely differing contrast between flares and quiescent emission in the *BeppoSAX* detectors (Figure 8 left) *in the framework of the stochastic-flare heating hypothesis*. We next need to investigate whether the larger flares themselves show a trend for hardening with increasing count rate. We emphasize again that we measure hardening by using two different effective area curves for two detectors, not by applying any spectral analysis.

There are two possible contributions that induce the non-proportionality between normalized LECS and MECS count rates in Fig. 8 (left): i) There is an intrinsic hardening for the larger flares, as suggested by the Feldman et al. and Aschwanden et al. relations. Thus, if the detector effective area curves vary differently across the relevant temperature range for LECS and MECS, we expect to see hardening signatures, i.e., non-proportionalities in Fig. 8. ii) The two detectors have, as argued above, different relative sensitivities to the quiescent emission compared to the (presumably hotter) large flares. To compare the flare count rates, the quiescent levels should be subtracted. We thus subtract a baseline quiescent count rate (0.105 ± 0.010 cts s $^{-1}$ for the LECS and 0.025 ± 0.005 cts s $^{-1}$ for the MECS). Fig. 8 (right) shows the relation between the residual count rates for LECS and MECS after the optimum subtraction. The slope of the best-fit line is $1.10_{-0.05}^{+0.06}$, i.e., there is still some hardening effect in the flare count rates. We show in the next subsection how the hardening of larger flares can explain the shallower flare energy distribution found for the MECS (compared to the LECS results).

6.3. Dependence on Spectral Range

The range of best-fit α agrees for all tests performed on the data from the *EUVE* DS and from the *BeppoSAX* LECS ($2.1 \lesssim \alpha \lesssim 2.4$). There seems to be a systematic shift of the MECS results relative to those from LECS, by approximately $\Delta\alpha = 0.2 - 0.4$ to lower α , i.e., the MECS distribution is shallower although this effect is only marginally significant.

For an isothermal plasma, a harder energy spectrum implies a higher plasma temperature. Feldman et al. (1995) reported a correlation for solar (plus a few stellar) flares between flare peak temperature T_0 and flare peak emission measure EM_0 (which scales approximately with the flare peak luminosity and, for constant decay times, with the total radiated flare

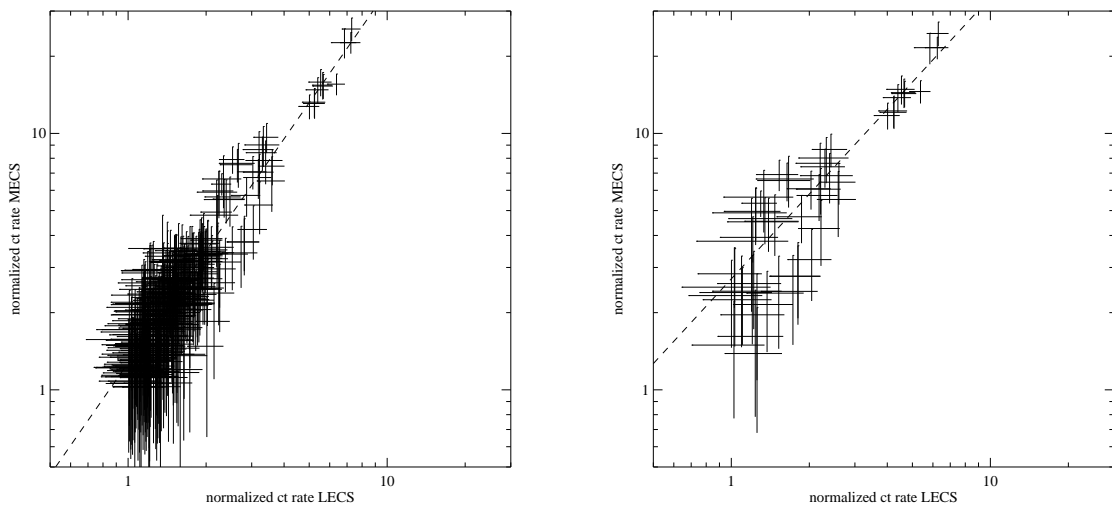


Fig. 8.— Correlation between simultaneous LECS and MECS count rates measured in 658 bins of 200 s duration each, for the complete light curve. The count rates were normalized with the quiescent values, and only normalized values exceeding unity are plotted. **Left:** All data included. Best-fit slope of the regression fit (dashed, using weights calculated from error bars): 1.45 ± 0.02 . – **Right:** Quiescent count rate level was subtracted before normalization. Best-fit slope of the regression fit (dashed): $1.10^{+0.06}_{-0.05}$.

energy). The relation is nearly exponential but can be reasonably approximated also by a power law over a limited range of temperatures,

$$\text{EM}_0 = aT_0^b \quad [\text{cm}^{-3}] \quad (3)$$

with $a \approx 2 \times 10^{13} \text{ cm}^{-3}\text{K}^{-b}$, $b \approx 5 \pm 1$ in the range of $T = 5 - 30 \text{ MK}$, and T measured in K. Aschwanden (1999) reports a power-law dependence between $T = 1 - 20 \text{ MK}$ with $b \approx 7$. The X-ray luminosity in general can be expressed as

$$L \approx \text{EM} \Lambda(T) = f \text{ EM} T^{-\phi} \quad (4)$$

with $\phi \approx 0.3$ over the above temperature range (for broad-band X-ray losses as derived in XSPEC or SPEX).

The count rate measured in a detector depends on the effective area curve and the incident X-ray spectrum which in turn depends on the plasma temperature T and the emission measure. We approximate the dominant X-ray emission at any one time as being emitted by an isothermal plasma of temperature T , with equation 3 satisfied, i.e., we identify any count rate at any given time with an individual flare at its peak and thus use its peak $\text{EM} = \text{EM}_0$ and peak $T = T_0$ for this estimate. Because we cannot perform time-resolved temperature analysis with the present data, we approximate the true flare energy distribution with the observed count distributions (i.e., $c \propto E$; the indices ℓ and m stand for LECS and MECS, respectively):

$$\frac{dN}{dc_\ell} \propto c_\ell^{-\alpha_\ell} \quad (5)$$

$$\frac{dN}{dc_m} \propto c_m^{-\alpha_m} \quad (6)$$

where the right-hand sides hold for the hypothesis that the energy distributions (i.e., the count rate distributions) are power laws. This approximation is acceptably good for outstanding flares, i.e., count rates well above the quiescent level, but breaks down near the quiescent level where numerous small flares may overlap.

We describe the dependence of the LECS and MECS count rates c_ℓ and c_m on temperature T and luminosity L with power-law approximations

$$c_\ell = c_{\ell,0} L T^{\gamma_\ell} \quad (7)$$

$$c_m = c_{m,0} L T^{\gamma_m} \quad (8)$$

where $c_{\ell,0}$ and $c_{m,0}$ are detector-related constants and γ_ℓ and γ_m describe the temperature sensitivity of the detector count rate. The γ values must be determined from the detector

effective areas. The expression $\mathcal{E}_\ell = c_\ell/L = c_{\ell,0}T^{\gamma_\ell}$ (similar for m) gives the observed *count rate per unit luminosity*, i.e., the efficiency of the detector to record a given luminosity in terms of a count rate, as a function of temperature.

We have folded a number of theoretical isothermal model spectra (in collisional equilibrium, as modeled in XSPEC [Arnaud 1996], and SPEX [Kaastra et al. 1996a]) with the detector response matrices for the DS, LECS, and MECS detectors to describe $\mathcal{E}_{\ell,m}(T)$. The count rates were derived across the range of sensitivity of the detector, and the L values have been evaluated for each T by integration of the model spectrum from 0.01–50 keV assuming a unit emission measure. The results are shown in Fig. 9. The efficiencies of the LECS and DS detectors are rather flat ($\gamma_\ell \approx 0$) at least in the region of interest, i.e., within approximately 0.5–5 keV. The LECS is least sensitive to changes in T and therefore *best recognizes flares of different temperatures with the least bias*. On the other hand, the efficiency of the MECS is a strong function of T below ~ 3 keV, with a rapid drop-off toward emission from cooler plasmas. Because of the dependence in equation 8, this implies that *weak flares are suppressed in the MECS, and strong flares are enhanced*. This is equivalent to an apparent decrease of α compared to the initial energy distribution.

To estimate this effect, we set $\gamma_\ell \equiv 0$ (for the temperature range of interest). The number distribution of flares (i.e., counts) in LECS count rate, dN/dc_ℓ , is therefore an unbiased approximation to the true flare radiative energy distribution dN/dE since $E \propto L$. Since

$$\frac{c_m}{c_\ell} = \frac{c_{m,0}}{c_{\ell,0}} T^{\gamma_m} = \frac{c_{m,0}}{c_{\ell,0}} \left(\frac{L}{af} \right)^{\gamma_m/(b-\phi)} = \frac{c_{m,0}}{c_{\ell,0}} \left(\frac{c_\ell}{af c_{\ell,0}} \right)^{\gamma_m/(b-\phi)} \quad (9)$$

(using equations 3 and 4) we obtain

$$c_m \propto c_\ell^{\gamma_m/(b-\phi)+1}. \quad (10)$$

Therefore,

$$\frac{dN}{dc_\ell} \equiv \frac{dN}{dc_m} \frac{dc_m}{dc_\ell} \propto \frac{dN}{dc_m} c_\ell^{\gamma_m/(b-\phi)}. \quad (11)$$

With equations 5 and 6 we find that

$$\alpha_\ell = \alpha_m \left(\frac{\gamma_m}{b-\phi} + 1 \right) - \frac{\gamma_m}{b-\phi}. \quad (12)$$

According to § 6.2, two components may be responsible for the apparent decrease of α ; we consider them to be limiting cases. (i) The hardening in Fig. 8 (left) could be attributed to the intrinsic spectral hardening toward larger energies of the visible flares only. We found $c_m \approx c_\ell^{1.45 \pm 0.02}$, hence $\gamma_m/(b-\phi) + 1 = 1.45$ and therefore $\gamma_m/(b-\phi) = 0.45$, so that $\alpha_\ell = 1.45\alpha_m - 0.45$. We find the highest confidence for $\alpha_\ell \approx 2.4$, hence we expect high

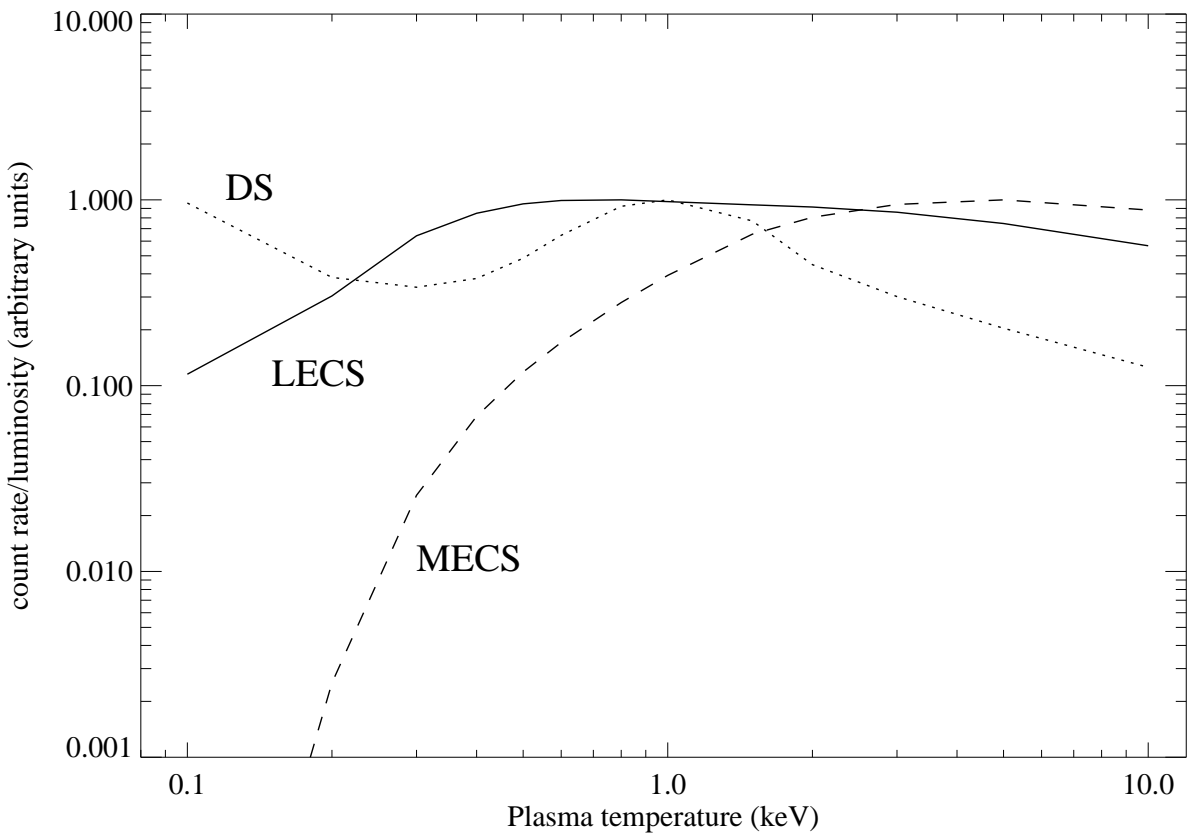


Fig. 9.— Efficiency (count rate/luminosity) as a function of (isothermal) plasma temperature for the *EUVE* DS, and the *BeppoSAX* LECS and MECS detectors (arbitrarily normalized).

confidence for $\alpha_m \approx 1.97 \pm 0.02$ (not including possible systematic errors of ± 0.1 as discussed above).

ii) Preceding subtraction of the quiescent count rate level both for LECS and MECS suggests (Figure 8 right) $c_m \approx c_\ell^{1.10(+0.08,-0.06)}$, hence $\gamma_m/(b-\phi) + 1 = 1.10$ and $\gamma_m/(b-\phi) = 0.1$, so that $\alpha_\ell = 1.10\alpha_m - 0.10$. We thus expect high confidence for $\alpha_m \approx 2.27 \pm 0.08$.

The expected difference $\alpha_\ell - \alpha_m \approx 0.13 - 0.43$ agrees with the measured difference of 0.2–0.4. We conclude that the hardening of flares with increasing total energy significantly affects the determination of α . While the LECS data provide, thanks to the flat efficiency curve, a relatively unbiased measure of the flare energy distribution (in terms of emitted energy), the MECS data consistently result in a harder appearance of the light curve, especially if the quiescent emission is included. We thus recognize the MECS result as biased by detector properties. As far as the DS results are concerned, they agree well with the LECS results, which is consistent with the relatively flat efficiency curve of the DS (Fig. 9).

Similar temperature bias has been discussed for solar coronal flare statistics derived from emission line flux ratios in the EUV range covering a narrow temperature range (Aschwanden & Charbonneau 2002; Aschwanden & Parnell 2002). One may extend this analysis to solar HXR data that have traditionally been used as a diagnostic of the total flare energy release (Lin et al. 1984). If the production of hard X-rays is more efficient in strong flares (the “Big Flare Syndrome”, Kahler 1982), then hard X-ray flare energy distributions are shallower than those constructed from soft X-ray or EUV data. There are at least indications that very small, low-temperature flares on the Sun are poor in radio emission, i.e., they produce high-energy electrons (important for the HXR production) less efficiently than larger flares (Krucker & Benz 2000).

6.4. The Emission Measure Distribution

We will now investigate effects of our hypothesis in the limiting case that all of the observed X-ray and EUV emission is due to superimposed stochastic-flare emission. In that case, we can use our α values to develop a crude model for the time-averaged EM distribution of the observed corona. We will estimate the amount of EM at a given temperature produced by a flare of any energy during its decay phase, and then integrate over the flare energy distribution. The time a flare spends at a given temperature is used as a weighting factor.

From equations 3 and 4 we obtain a relation between the flare peak temperature T_0 and

its peak luminosity L_0 ,

$$T_0 = \left(\frac{L_0}{af} \right)^{1/(b-\phi)}. \quad (13)$$

Note that for decay times τ independent of E , the peak luminosity follows the same power-law as the total radiated energy:

$$\frac{dN}{dL_0} = k\tau^{-\alpha+1}L_0^{-\alpha} \quad (14)$$

(since $E = L_0\tau$). However, we will also investigate the case in which τ varies with the flare energy, namely

$$\tau = \tau_0 E^\beta \quad (15)$$

(where $\beta \geq 0$ is assumed, and τ_0 is a constant adjusted to the larger detected flares) in which case

$$\frac{dN}{dL_0} = \frac{dN}{dE} \frac{dE}{dL_0} = k'L_0^{-(\alpha-\beta)/(1-\beta)}. \quad (16)$$

where the constant $k' = k\tau_0^{(1-\alpha)/(1-\beta)}/(1-\beta) > 0$ as long as $\beta < 1$ (which can be reasonably assumed). Since we neglect the short rise time of the flare, our flare light curves are described by their exponential decay at $t \geq 0$,

$$L(t) = L_0 e^{-t/\tau}. \quad (17)$$

From hydrodynamic modeling, theory and observations, it is known that during the flare decays $T \propto n^\zeta$, where n is the plasma density (Reale et al. 1993). The parameter ζ is usually found between 0.5 and 2 (Reale et al. 1993). A value of $\zeta = 2$ holds if the heating source abruptly turns off at flare peak, and the flare cools freely via radiation and conduction. A low value of ζ indicates sustained heating during the decay phase. For example, for $\zeta \approx 0.5 - 0.7$ the decay time of the flare emission is 2–4 times slower than predicted for a freely cooling magnetic loop (Reale et al. 1997). Solar observations of moderate flares with *SMM* show ζ between $\sim 0.5 - 2$ (Sylwester et al. 1993), although Reale et al. (1997) find a predominance of values around $\sim 0.3 - 0.7$, i.e., flares with sustained heating. For larger stellar flares, there is much evidence for small ζ as well: Reale & Micela (1998) find a flare decay that is $\gtrsim 2$ times slower than for a freely cooling loop; Favata et al. (2000a) find $\zeta = 0.56 \pm 0.04$ for a flare on EV Lac, and Favata et al. (2000b) report $\zeta = 0.48 \pm 0.06$ for a flare on AD Leo; Güdel et al. (2001b) find $\zeta = 0.95 \pm 0.15$ for a moderate flare on AB Dor. Since, under the assumption of constant volume, the emission measure scales with n^2 , we have

$$\frac{T}{T_0} = \left(\frac{\text{EM}_T}{\text{EM}_0} \right)^{\zeta/2}. \quad (18)$$

From equations 4, 17 and 18, we obtain the temperature time evolution

$$T(t) = T_0 e^{-t/(2\tau[1/\zeta - \phi/2])} \quad (19)$$

where we require $\phi < 2/\zeta$ for a temperature decay (this is usually fulfilled as $\phi \approx 0$ and $2/\zeta \geq 1$). The emission measure EM_T at temperature T for this particular flare is, from equations 18 and 3,

$$\text{EM}_T = aT_0^{b-2/\zeta} T^{2/\zeta} \quad (20)$$

and this expression must be weighted with the fractional duration (out of the total observing time P) during which the flare resides within the logarithmic temperature interval $[\ln T, \ln T + d\ln T]$, i.e., dt/P . The emission measure contribution EM_T thus counts in full if it is constantly present during the observing time. The duration dt is obtained by differentiating equation 19 (we only require the absolute value of $d\ln T$), so that the weight is

$$\frac{dt}{P} = \frac{2\tau}{P} \left(\frac{1}{\zeta} - \frac{\phi}{2} \right) |d\ln T|. \quad (21)$$

Multiplying equations 20 and 21 and substituting all expressions, we find the weighted contribution of a flare with peak luminosity L_0 to the emission measure at temperature T ,

$$\begin{aligned} \delta(\text{EM}_T) &= \frac{2a\tau_0^{1/(1-\beta)}}{P} \left(\frac{1}{\zeta} - \frac{\phi}{2} \right) \\ &\times \left(\frac{L_0}{af} \right)^{(b-2/\zeta)/(b-\phi)} L_0^{\beta/(1-\beta)} T^{2/\zeta} |d\ln T| \\ &= c L_0^{(b-2/\zeta)/(b-\phi)+\beta/(1-\beta)} T^{2/\zeta} |d\ln T|. \end{aligned} \quad (22)$$

where all constant factors are absorbed in c . It is positive as long as $\phi < 2/\zeta$ (from equation 21 and as required for equation 19). Expression 22 must be integrated over N in the distribution 16 for all possible peak luminosities L_0 to obtain the differential emission measure distribution (DEM), i.e.,

$$\begin{aligned} Q(T) &= \frac{d(\text{EM})}{|d\ln T|} = \int_{L_1}^{L_2} \frac{\delta(\text{EM}_T)}{|d\ln T|} \frac{dN}{dL_0} dL_0 \\ &= ck'T^{2/\zeta} \int_{L_1}^{L_2} L_0^{(b-2/\zeta)/(b-\phi)-(\alpha-2\beta)/(1-\beta)} dL_0 \\ &= \frac{c'T^{2/\zeta}}{(\text{exponent})} L_0^{(b-2/\zeta)/(b-\phi)-(\alpha-2\beta)/(1-\beta)+1} \Big|_{L_1}^{L_2} \end{aligned} \quad (23)$$

where $c' = ck'$ is again a numerical constant that is > 0 if $\beta < 1$ (which is fulfilled; also note that $\beta \neq 1$ is required; see equation 16). The denominator “(exponent)” is identical to the

exponent of L_0 which we assume is negative so that large but rare flares do not dominate the average emission measure distribution. This holds for reasonable choices of b , β , and ϕ for a given α but needs to be checked in individual cases. Then, the upper integration limit can be set to $L_2 = \infty$ as the corresponding term converges to zero, and the complete expression 23 remains positive. For the lower limit L_1 , there are two cases. i) For a given T , there is a smallest flare that reaches this temperature at its peak, i.e., $T = T_0$, and this flare then has a peak luminosity given by equation 13, i.e., $L_0 = afT_0^{b-\phi}$. ii) Since $\alpha > 2$, a lower energy cut-off of the flare energy distribution is required. Flares with energies below this limit E_{\min} are assumed to be unimportant for the heating. The minimum radiated flare energy corresponds to a minimum peak luminosity $L_{\min} = E_{\min}/\tau$ and was reported in Table 4. We therefore require

$$L_1(T) = \max(afT^{b-\phi}, L_{\min}). \quad (24)$$

Consequently, there are two temperature regimes, depending on whether the first or second expression applies. From equation 23, we obtain

$$Q \propto T^{2/\zeta} \quad , afT^{b-\phi} \leq L_{\min} \quad (25)$$

$$\propto T^{-(b-\phi)(\alpha-2\beta)/(1-\beta)+2b-\phi} \quad , afT^{b-\phi} > L_{\min} \quad (26)$$

The EM distribution thus rises with a slope of $2/\zeta$ from low temperatures toward a turnover, and then drops again with a power-law exponent that depends on the flare energy distribution index α . The turnover occurs where $afT^{b-\phi} = L_{\min}$. Note that for $\zeta = 0.3 - 0.7$ (Reale et al. 1997), $Q \propto T^{3-7}$ which is much steeper than the prediction from a quasi-static loop model but agrees well with measurements of the DEM of the active K star ϵ Eri (Laming et al. 1996) and of the late G star ξ Boo A (Drake & Kashyap 2001). The DEM thus provides another important diagnostic for flare-heated coronae: i) The high- T slope of the distribution can be used to determine α ; ii) the low- T slope gives information on the heating time-scale of flares during their decay; and iii) the peak indicates the turnover energy from a steep to a shallow flare energy power-law. – We briefly discuss two cases, for which we use $\alpha = 2.2$.

i) For τ independent of flare energy, $\beta = 0$. Our simulations required lowest energies corresponding to peak luminosities as low as a few times 10^{25} erg s $^{-1}$; we assume $L_{\min} = 10^{25} - 10^{26}$ erg s $^{-1}$. The cooling losses per unit emission measure are only weakly dependent on temperature in the X-ray range (0.1–10 keV), namely $\Lambda \approx 2 \times 10^{-23}$ erg cm 3 s $^{-1}$ (determined from a MEKAL model in XSPEC using our best-fit abundance for Fe). The peak EM required for such a flare is thus $5 \times 10^{47} - 5 \times 10^{48}$ cm $^{-3}$, which, from the Feldman et al. relation, corresponds to a temperature of about 9–16 MK, with considerable scatter. This is indeed the temperature regime of peak EM in the emission measure distribution. It is, however, unlikely that the flare energy distribution is limited by an abrupt cut-off at low energies.

Rather, the power-law index is likely to become smaller at lower energies so that smaller flares become less relevant for heating. We therefore set the turnover temperature arbitrarily at ~ 7 MK, in agreement with the observational DEM. The high- T part of the DEM is thus determined mainly by plasma between 10–40 MK (see Figure 10). The Feldman et al. relation is best fitted by $b = 6 \pm 1$ in that regime, and the cooling function (as calculated in XSPEC for an Fe abundance of 0.54 times solar photospheric) has an average slope of $\phi = 0.3$ in that range. We propose to set $\zeta = 0.5 - 1$, in the light of the above discussion of published values. We thus find $Q \propto T^{3 \pm 1}$ for the low- T part of the emission measure distribution, and $Q \propto T^{b(2-\alpha)-\phi(1-\alpha)} = T^{-0.2b+0.36} = T^{-0.84 \pm 0.20}$ for the high- T part. This model DEM is shown in Fig. 10 (dashed) together with a quiescent DEM (dotted) and a DEM from all data (solid), both derived from LECS and MECS (using the polynomial and the regularization method as described in Kaastra et al. 1996a). Clearly, including the visible flares fills in more emission measure at temperatures between 20–50 MK, as expected. This explicitly confirms that the high- T DEM is largely related to flaring emission. The fact that the quiescent DEM in Figure 10 still contains plasma at ~ 40 MK is likely to be due to the inclusion of many small flare peaks not cut out for this fit. The reconstructed DEM has limited quality given the restricted resolution of the *BeppoSAX* detectors, but the comparison with the theoretical DEMs is suggestive except for the presence of a cool peak at 0.15 keV.

ii) We previously discussed the possibility that $\beta = 0.25$. Again, we set $\phi = 0.3$ and $\zeta = 0.5 - 1$. Then, the low- T slope remains the same, 3 ± 1 , and the high- T DEM varies like $Q \propto T^{-0.267b+0.38} = T^{-1.22 \pm 0.27}$, i.e., quite similar to case (i).

7. Conclusions

We have investigated the role of statistical flares in coronal heating of magnetically active stars. Long observations of AD Leo were obtained in order to maximize flare statistics. Flares have been suspected to play an important role in coronal energy release and subsequent impulsive heating of chromospheric material to high temperatures. Chromospheric evaporation induced by chromospheric overpressure lifts the hot plasma into the corona where it fills closed magnetic loops. Since (solar) flares are always related not only to an increase in emission measure but to a significant increase in the average plasma temperature, they are natural candidates to heat perhaps all of the detected coronal plasma. Recent progress in solar physics (Krucker & Benz 1998; Aschwanden et al. 2000; Parnell & Jupp 2000) has added new momentum to this hypothesis.

Active (but quiescent) stellar coronae exhibit a number of features unknown to the non-flaring Sun but suspiciously reminiscent of solar (or stellar) flares: i) Very high temperatures

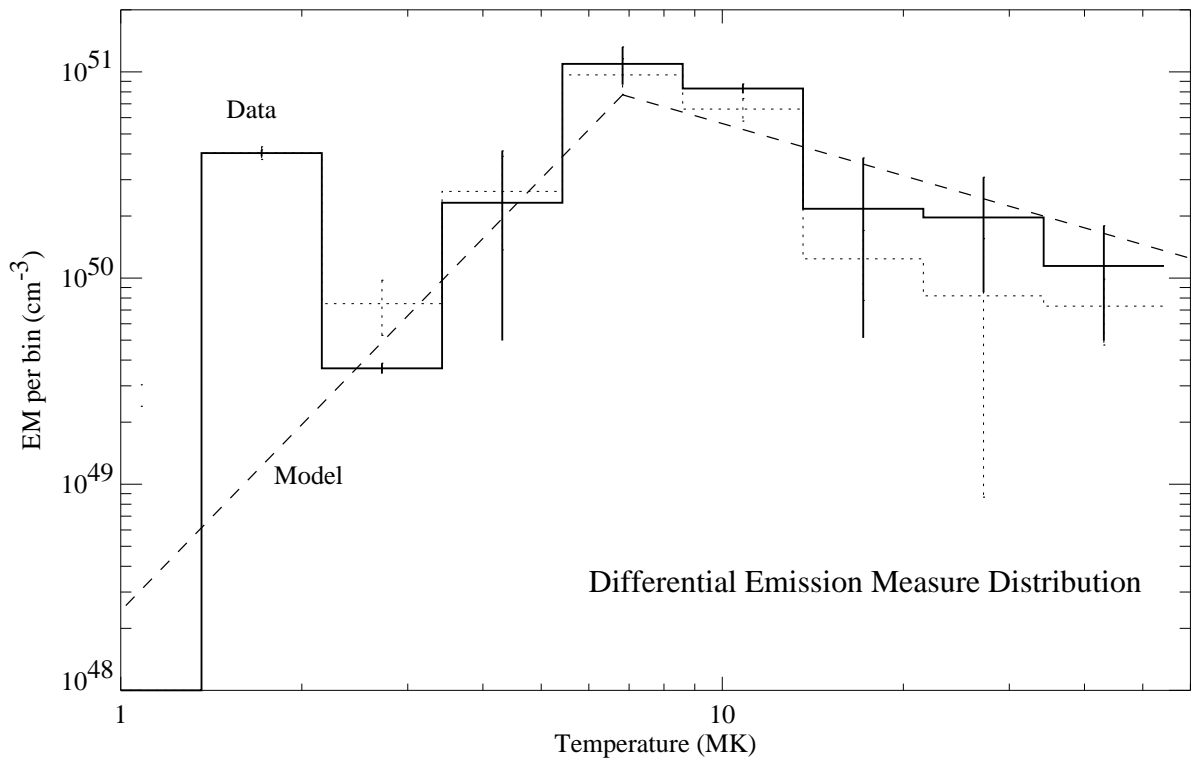


Fig. 10.— Emission measure distribution of the quiescent emission of AD Leo, derived from the combined *BeppoSAX* LECS and MECS data. The bins are equidistant in $d\log T$. The emission measures are averages derived from a polynomial fit and a regularization method (for details, see Kaastra et al. 1996b). The dashed lines illustrate the approximate slopes of the DEM expected from a superposition of flares (arbitrarily adjusted in EM_{peak}).

up to 2–3 keV, similar to temperatures of large solar flares; ii) accompanying, strong non-thermal gyrosynchrotron radio emission attributed to relativistic electrons accelerated in the initial phase of the flare energy release (Güdel 1994 and references therein) ; iii) high densities ($\gtrsim 10^{10} \text{ cm}^{-3}$) reminiscent of (solar) flare densities (Güdel et al. 2001a,b); iv) "anomalous" elemental abundances tentatively ascribed to the action of flares, perhaps analogs to solar Ne- and S-rich flares (Brinkman et al. 2001; Drake et al. 2001); v) and finally, the presence of a large number of strong flares, where the rate of detected flares correlates with the quiescent emission level (Audard et al. 2000).

We have studied the distribution of EUV and X-ray flares in energy, seeking power laws of the form $dN/dE = kE^{-\alpha}$ where k is the normalization of the distribution and α determines the steepness of the distribution. We have applied two methods, one based on the count rate distribution of binned data, and the second related to the distribution of arrival-time differences of the original photon lists (only for *EUVE*). Despite the fundamentally different approaches, the results of both methods are in excellent agreement for the *EUVE* data and indicate $\alpha = (2.1 - 2.3) \pm 0.1$. Simultaneous X-ray observations obtained with the *BeppoSAX* LECS were treated with the first method. The results again overlap with the *EUVE* results, namely $\alpha = 2.4 \pm 0.2$. Only the MECS data show somewhat shallower distributions, with $\alpha = (2.0 - 2.2) \pm 0.2$ which can be explained by the harder sensitivity range of the MECS detector, and detection bias in terms of flare temperatures. Our results are compatible with the findings of Audard et al. (2000) who applied a flare identification algorithm to explicitly record flares and to measure their energies. They are further supported by the findings of Kashyap et al. (2002) who study further active stars with the *EUVE* DS. At first sight, our α values support a model in which the complete coronae are heated by a statistical distribution of flares, involving flares with energies down to a few times 10^{29} erg (of radiated energy). Also, a model EM distribution based on the superposition of flares of different peak temperatures is compatible with the observed EM distribution. However, before we can conclude that flares play an important role in the coronal heating process, we should keep in mind the following caveats that stellar observations of the present quality are invariably subject to:

(A) All EUV and X-ray observations refer to the radiated energy from the hot plasma. There is considerable ignorance of other energy partitions that also contribute to the flare energy budget (Wu et al. 1986): Kinetic energy of the upstreaming plasma; potential energy of the lifted plasma; energy in waves; energy in accelerated particles; and energy released at longer wavelengths. To interpret our results physically, we adopt the following working hypothesis: i) The energy initially released in energetic particles is largely thermalized in the chromospheric evaporation process. ii) The remaining energy (kinetic and potential) is eventually thermalized (e.g., when material drops back to the chromosphere). iii) All

thermal energy is eventually radiated away during the cooling processes. We emphasize that this applies also to all energy that is conducted from the coronal loops downwards. This energy is radiated by the chromosphere. iv) The fraction of the radiative energy released in the X-ray range is similar for all flares.

While points i)–iii) are supported by observations (Dennis 1985) and by numeric simulations (e.g., Nagai & Emslie 1984; Antonucci et al. 1987), point iv) is relatively difficult to assess. Clearly, a considerable part of the energy is lost at UV wavelengths not accessible to our observations. The tendency of the flare temperature to increase with overall flare energy (Feldman et al. 1995; Aschwanden 1999) would suggest that smaller flares lose a larger fraction of their energy outside the EUV/X-ray regime. This is, however, of little relevance for us: All flares considered here are quite large, with probable peak temperatures (according to the Feldman et al. relation) exceeding 20 MK; even the quiescent emission shows its peak EM between 5–10 MK (Table 3). Hudson (1991) reports that approximately 2/3 of the total radiant energy of a solar flare are emitted in soft X-rays. The total, long-term average energy loss in optical U band flares is linearly correlated with the average X-ray losses in active stars (Doyle & Butler 1985). If we missed a population of very small flares with very low temperatures (e.g., comparable to microflares in the Sun), then they would simply add to the flare distribution on the low-energy side, i.e., our distributions would become steeper still, making small flares even more crucial for the total energy release. Further, the measured average thermal energy input (“heating rate”) during a solar flare scales linearly with the radiative loss rate in X-rays (Aschwanden et al. 2000).

Finally, from the phenomenological point of view adopted in the present study, the relation between losses in the X-rays/EUV and those at longer wavelengths can be ignored altogether if we keep with our goal of modeling the *observed coronal* emission. The latter is clearly dominated by X-ray/EUV radiation. If we successfully explain the total X-ray/EUV emission by the radiation of a statistical ensemble of flares, then this simply implies that there is no significant additional *coronal* component. Although there may be additional energy release at lower temperatures (i.e., at chromospheric levels), this becomes irrelevant for the question of *coronal* heating.

(B) The power-law distribution of flares may change spatially on the star. Stellar observations unavoidably treat the corona as an average structure. The recent solar results with $\alpha > 2$ were obtained in regions of the quiet Sun while most larger flares occur in active regions. It may, however, be interesting to mention that an observation of a *single* solar X-ray bright point resulted in a power-law index similar to those obtained from the whole Sun (Shimojo & Shibata 1999).

(C) The power-law distributions may also vary in time. Bai (1993) and Bromund,

McTiernan, & Kane (1995) find a 154 d periodicity in which α changes by $\sim 0.2 - 0.4$ in solar data. There may also be a dependence on the overall magnetic activity level that varies with the (cyclic or irregular) “magnetic activity cycle”. This latter conjecture is, however, not supported by the solar studies of Feldman et al. (1997) and Lu & Hamilton (1991). We note that we found different values for α depending on whether or not the early part of the DS observation (containing a large flare) was included.

(D) Although we have used a rather long observing time series (27.3 days of coverage with *EUVE*, referring to segment I–IV), some chance coincidence, like the very large flare at the beginning of the observation, may introduce considerable systematic bias. We have investigated the role of this large flare on the result for α and found indeed that its selective inclusion/exclusion can shift the optimum value by $\Delta\alpha \approx 0.1$.

(E) There may be high-energy cut-offs (“roll-overs”; Kucera et al. 1997) related to the maximum energy that can be liberated in stellar active regions. In a limited set of observations with a limited dynamic range (ratio of strongest to weakest detected flares, also depending on the noise level), the deficit of flares close to the high-energy cut-off (because of their small occurrence rate) can induce a steepening of a power law. A consequent shallower continuation of the distribution toward flares below our detection limit would contribute less energy than estimated with our single power-law approach. The present data do not allow us to judge on the presence or absence of high-energy cut-offs. The good representation by single-power-law flare distributions does presently not argue for their presence. The continuation of the power law from detected flares to energies below the detection threshold has been explicitly assumed in our energy estimates, and this is no different from any previous (solar or stellar) study. For sufficiently small energies, the large number of small flares involved begin to overlap in time (the “confusion limit”, already evident in our light curves). They can no longer be measured individually unless spatial resolution is available.

(F) Appreciable non-flare contributions to the EUV/X-ray variability are possible (e.g., evolution of non-flaring active regions, newly emerged magnetic regions, rotational modulation of active regions). They would normally add to the low-level variability and may thus tend to steepen the count rate distributions.

Despite these caveats, some of which will be difficult or impossible to avoid in future observations, we presently see no compelling argument against our basic finding, namely, that flares statistically contribute an important part to the overall coronal radiative losses, and that they are therefore good candidates for the coronal heating process *per se* in magnetically active stars.

Our values for α are very similar to those measured for microflares in the Sun (Krucker &

Benz 1998; Parnell & Jupp 2000) despite the 6 orders of magnitude larger energies involved. This factor in energy may partly reflect the level of magnetic activity. If so, then the role played by microflares in the Sun is played by the much larger flares relevant here in active stellar coronae.

We find independent support for flare heating of active stellar coronae in their coronal emission measure distribution. By statistically co-adding flaring emission measures by weighting them with the dwell time at a given temperature, we derived an analytical expression for the differential emission measure distribution. The DEM is characterized by a steeply rising low-temperature part and a falling high-temperature part. The slopes and the turnover temperature are in principle determined by the flare energy power-law index α , the low-energy break in the distribution, and the flare heating parameter ζ during the flare decay. Previously published DEMs of active stars (e.g., Laming et al. 1996; Drake & Kashyap 2001) and the DEM derived here show characteristic shapes that are compatible with our expression but are not supported by quasi-static loop models. We suggest that the coronal DEMs directly reflect the operation of heating and cooling mechanisms during stochastic flares (Güdel 1997; Güdel et al. 1997).

We conclude this presentation by emphasizing two observational circumstances: i) It may be pivotal in which energy range relevant for coronal losses the observations are made. Observations that exclusively record the harder part of soft X-rays selectively favor detections of large flares and suppress the relevance of low-energy flares (due to the Feldman et al. relation; see also discussion in Porter et al. 1995). As is to be expected from the flare-heating hypothesis, the quiescent emission is comparatively soft and is therefore also underrepresented in hard observations. We have marginally found this effect in our MECS observations. One may wonder whether a similar effect exists for non-thermal hard X-rays often used for solar flare energy statistics. If they are generated overproportionally in larger flares (as suggested by the “Big Flare Syndrome”, Kahler 1982, but also by recent observations finding that microflares are radio-poor, i.e., relatively weak in the production of accelerated particles, Krucker & Benz 2000) then the statistical distributions may be biased toward too low α . We have selected the energy range in which the dominant fraction of the coronal flare energy is radiated. Also, the efficiency (ratio between observed count rate and incident flux) of the DS and the LECS detectors shows only a weak temperature dependence, i.e., the observations are equally sensitive to plasma over a wide range of relevant temperatures. ii) The power-law distribution may depend on the flare energy range considered. There are indications in solar observations to this effect, and we can safely state that the power laws found here cannot be extrapolated to arbitrary energies: There must be a low-energy break (possibly changing to a shallower distribution) in order to confine the total radiated power, and there must be a high-energy limit, corresponding to the largest

physically possible flares.

The authors thank the referee, Alexander Brown, for thoughtful and constructive comments on the original manuscript. We thank the *EUVE* and *BeppoSAX* staff for their generous support of our observing campaign. The PSI group (MG, MA) acknowledges partial financial support by the Swiss National Science Foundation (grants 2100-049343 and 2000-058827). JJD and VLK acknowledge support from NASA grants and the Chandra X-Ray Center during the course of this research.

REFERENCES

Ambruster, C. W., Sciortino, S., & Golub, L. 1987, *ApJ*, 65, 273

Anders, E., & Grevesse, N. 1989, *Geochim. Cosmochim. Acta*, 53, 197

Antonucci, E., Dodero, M. A., Peres, G., Serio, S., & Rosner, R. 1987, *ApJ*, 322, 522

Arnaud, K. A. 1996, in *ASP Conf. Ser.* 101, *Astronomical Data Analysis Software and Systems V*, ed. G. Jacoby & J. Barnes (San Francisco: ASP), 17

Aschwanden, M. J. 1999, *Sol. Phys.*, 190, 233

Aschwanden, M. J., & Charbonneau, P. 2002, *ApJ*, 566, L59

Aschwanden, M. J., & Parnell, C. E. 2002, *ApJ*, 572, 1048

Aschwanden, M. J., Tarbell, T. D., Nightingale, R. W., Schrijver, C. J., Title, A., Kankelborg, C. C., Martens, P. C. H., & Warren, H. P. 2000, *ApJ*, 535, 1047

Audard, M., Güdel, M., Drake, J. J., & Kashyap, V. 2000, *ApJ*, 541, 396

Audard, M., Güdel, M., & Guinan, E. F. 1999, *ApJ*, 513, L53

Bai, T. 1993, *ApJ*, 404, 805

Benz, A. O. 1994, *Lecture Notes in Physics*, 444, 1

Boella, G., Butler, R. C., Perola, G. C., Piro, L., Scarsi, L., & Bleeker, J. A. M. 1997a, *A&AS*, 122, 299

Boella, G., Chiappetti, L., Conti, G., et al. 1997b, *A&AS*, 122, 327

Brinkman, A. C., et al. 2001, *A&A*, 365, L324

Bromund, K. R., McTiernan, J. M., & Kane, S. R. 1995, *ApJ*, 455, 733

Collura, A., Pasquini, L., & Schmitt, J. H. M. M. 1988, *A&A*, 205, 197

Crosby, N. B., Aschwanden, M. J., & Dennis, B. R. 1993, *Sol. Phys.*, 143, 275

Datlowe, D. W., Elcan, M. J., & Hudson, H. S. 1974, *Sol. Phys.*, 39, 155

Dennis, B. R. 1985, *Sol. Phys.*, 100, 465

Dere, K. P., Bartoe, J.-D. F., & Brueckner, G. E. 1989, *Sol. Phys.*, 123, 41

Doyle, J. G., & Butler, C. J. 1985, *Nature*, 313, 378

Drake, J. F. 1971, *Sol. Phys.*, 16, 152

Drake, J. J., Brickhouse, N. S., Kashyap, V., Laming, J. M., Huenemoerder, D. P., Smith, R., & Wargelin, B. J. 2001, *ApJ*, 548, L81

Drake, J. J., & Kashyap, V. 2001, *ApJ*, 547, 428

Favata, F., Micela, G., & Reale, F. 2000b, *A&A*, 354, 1021

Favata, F., Reale, F., Micela, G., Sciortino, S., Maggio, A., & Matsumoto, H. 2000a, *A&A*, 353, 987

Feldman, U., Doschek, G. A., & Klimchuk, J. A. 1997, *ApJ*, 474, 511

Feldman, U., Laming, J. M., & Doschek, G. A. 1995, *ApJ*, 451, L79

Fiore, F., Guainazzi, M., & Grandi, P. 1999, *Cookbook for BeppoSAX NFI Spectral Analysis*, version 1.2: 7 January 1999

Frontera, F., Costa, E., & dal Fiume, D. 1997, *A&AS*, 122, 357

Gary, D. E., Hartl, M. D., & Shimizu, T. 1997, *ApJ*, 477, 958

Giampapa, M. S., Rosner, R., Kashyap, V., Fleming, T. A., Schmitt, J. H. M. M., & Bookbinder, J. A. 1996, *ApJ*, 463, 707

Güdel, M. 1994, *ApJS*, 90, 743

Güdel, M. 1997, *ApJ*, 480, L121

Güdel, M., et al. 2001b, *A&A*, 365, L336

Güdel, M., Audard, M., Magee, H., Franciosini, H., Grosso, N., Cordova, F. A., Pallavicini, R., & Mewe, R. 2001a, *A&A*, 365, L344

Güdel, M., Benz, A. O., Schmitt, J. H. M. M., & Skinner, S. L. 1996, *ApJ*, 471, 1002

Güdel, M., Guinan, E. F., & Skinner, S. L. 1997, *ApJ*, 483, 947

Haisch, B., & Schmitt, J. H. M. M. 1996, *PASP*, 108, 113

Hudson, H. S. 1991, *Sol. Phys.*, 133, 357

Hudson, H. S., Peterson, L. E. & Schwartz, D. A. 1969, *ApJ*, 157, 389

Ionson, J. A. 1985, *Sol. Phys.*, 100, 289

Kaastra, J. S., Mewe, R., Liedahl, D. A., Singh, K. P., White, N. E., & Drake, S. A. 1996b, *A&A*, 314, 547

Kaastra, J. S., Mewe, R., & Nieuwenhuijzen H. 1996a, in UV and X-Ray Spectroscopy of Astrophysical and Laboratory Plasmas, ed. K. Yamashita & T. Watanabe, (Tokyo: Univ. Acad. Press), 411

Kahler, S. W. 1982, *J. Geophys. Rev.*, 87, 3439

Kashyap, V. & Drake, J. J. 1999, *ApJ*, 524, 988

Kashyap, V., Drake, J. J., Güdel, M., & Audard, M. 2002, *ApJ*, in press

Krucker, S., & Benz, A. O. 1998, *ApJ*, 501, L213

Krucker, S., & Benz, A. O. 2000, *Sol. Phys.*, 191, 341

Kucera, T. A., Dennis, B. R., Schwartz, R. A., & Shaw, D. 1997, *ApJ*, 475, 338

Laming, J. M., Drake, J. J., & Widing, K. G. 1996, *ApJ*, 462, 948

Lin, R. P., Schwartz, R. A., Kane, S. R., Pelling, R. M., & Hurley, K. 1984, *ApJ*, 283, 421

Lu, E. T., & Hamilton, R. J. 1991, *ApJ*, 380, L89

Lu, E. T., & Hamilton, R. J., McTiernan, J. M., & Bromund, K. R. 1993, *ApJ*, 412, 841

Malina, R. F., & Bowyer, S. 1991, in Extreme-Ultraviolet Astronomy, ed. R. F. Malina & S. Bowyer, (New York: Pergamon), 391

Mullan, D. J., & Cheng, Q. Q. 1994, *ApJ*, 420, 392

Narain, U., & Ulmschneider, P. 1990, *Space Sci. Rev.*, 54, 377

Nagai, F., & Emslie, A. G. 1984, *ApJ*, 279, 896

Osten, R. A., & Brown, A. 1999, *ApJ*, 515, 746

Pallavicini, R., Tagliaferri, G., & Stella, L. 1990, *A&A*, 228, 403

Parker, E. N. 1988, *ApJ*, 330, 474

Parmar, A. N., Guainazzi, M., & Oosterbroek, T. 1999, *A&A*, 345, 611

Parmar, A. N., Martin, D. D. E., & Baudaz, M. 1997, *A&AS*, 122, 309

Parnell, C. E., & Jupp, P. E. 2000, *ApJ*, 529, 554

Porter, J. G., Fontenla, J. M., & Simnett, G. M. 1995, *ApJ*, 438, 472

Reale, F., & Micela, G. 1998, *A&A*, 334, 1028

Reale, F., Betta, R., Peres, G., Serio, S., & McTiernan, J. 1997, *A&A*, 325, 782

Reale, F., Serio, S., & Peres, G. 1993, *A&A*, 272, 486

Robinson, R. D., Carpenter, K. G., & Percival, J. W. 1999, *ApJ*, 516, 916

Robinson, R. D., Carpenter, K. G., Percival, J. W., & Bookbinder, J. A. 1995, *ApJ*, 451, 795

Robinson, R. D., Linsky, J. L., Woodgate, B. E., & Timothy, J. G. 2001, *ApJ*, 554, 368

Sciortino, S., Maggio, A., Favata, F., & Orlando, S. 1999, *A&A*, 342, 502

Serio, S., Peres, G., Vaiana, G. S., Golub, L., & Rosner, R. 1981, *ApJ*, 243, 288

Shimizu, T. 1995, *PASJ*, 47, 251

Shimojo, M., & Shibata, K. 1999, *ApJ*, 516, 934

Skumanich, A. 1985, *Aust. J. Phys.*, 38, 971

Stępień, K., & Ulmschneider, P. 1989, *A&A*, 216, 139

Sylwester, B., Sylwester, J., Serio, S., Reale, F., Bentley, R. D., & Fludra, A. 1993, *A&A*, 267, 586

Vlahos, L., Georgoulis, M., Kluiving, R., & Paschos, P. 1995, *A&A*, 299, 897

Wood, B. E., Harper, G. M., Linsky, J. L., & Dempsey, R. C. 1996, *ApJ*, 458, 761

Wu, S. T., et al. 1986, in *Energetic Phenomena on the Sun. SMM Flare Workshop Proceedings*, NASA CP 2439, 5-1

Zirker, J. B. 1993, *Sol. Phys.*, 148, 43